2019-01-01

Assessing Delamination Of Concrete Bridge Decks With Aging In Arid Regions Using Nondestructive Testing Methods

Melissa Escalante
University of Texas at El Paso, miescalante@miners.utep.edu

ASSESSING DELAMINATION OF CONCRETE BRIDGE DECKS WITH AGING IN ARID REGIONS USING NONDESTRUCTIVE TESTING METHODS

MELISSA ESCALANTE

Master's Program in Civil Engineering

APPROVED:

Soheil Nazarian, Ph.D., Chair

Danniel Rodriguez, Ph.D.

Diane Doser, Ph.D.

Charles Ambler, Ph.D.
Dean of the Graduate School

Dedication

I would like to dedicate this work to the loving memory of my father, Ramon Escalante, whose ***unconditional love, care, and courage*** during his fifteen years in my life gave me the strength to conclude my educational path.

ASSESSING DELAMINATION OF CONCRETE BRIDGE DECKS WITH AGING IN ARID REGIONS USING NONDESTRUCTIVE TESTING METHODS

by

MELISSA ESCALANTE, EIT, BSCE

THESIS

Presented to the Faculty of the Graduate School of

The University of Texas at El Paso

in Partial Fulfillment

of the Requirements

for the Degree of

MASTER OF SCIENCE

Department of Civil Engineering

THE UNIVERSITY OF TEXAS AT EL PASO

May 2019

Acknowledgments

I offer my deepest gratitude to my professor and graduate research supervisor Dr. Soheil Nazarian, for his guidance, patience, and assistance during my graduate studies. His mentorship and essential advice gave me the necessary tools to attain a successful career. I would like to also thank Sergio Rocha and Dr. Prajwol Tamrakar for their help, time and concern in the completion of this work. I also thank the rest of my thesis committee, Dr. Danniel Rodriguez and Dr. Diane Doser, for their participation and assistance in the development and completion of this work. I would like to thank the support from faculty at The University of Texas at El Paso (UTEP) Center for Transportation Infrastructure Systems (CTIS), especially the center director Dr. Imad Abdallah, and students Benjamin Arras, Alejandro Gomez, and Luisa Morales for their help and support during the experimental procedures.

I would like to extend my gratitude to my friends Diana Cabrera, Alejandra Escajeda, Luis Lemus, Sofia Martin, Yair Morales, John Padilla, Juan Carlos Salcido, Maria Torres, Paola Villescas and Paloma Zamarripa for their time, constant support and encouragement for the completion of this work.

Most importantly I would like to thank my mother, Martha Escalante, grandmother Maria Alicia Clarke, and my siblings Rodrigo and Cynthia Escalante for their continued concern, strength, patience and support throughout the completion of my education.

Abstract

Bridge decks usually experience deterioration at a more rapid pace than other infrastructure components due to the heavy traffic loads and environmental conditions that the deck sustains. Delamination within concrete bridge decks accelerates due to water and deicing salts penetrating the concrete; resulting in the corrosion of reinforcing steel. The corrosion of rebar may result in a fracture parallel to the surface of the concrete structure at the top of the reinforcement layer. The delamination is then subjected to expansion over a large span; risking the overall stability of the structural element. Health monitoring of concrete bridge decks is therefore necessary for determining the condition of structural elements and to prescribe appropriate preservation, repair, rehabilitation or replacement. Nondestructive testing (NDT) methods have shown promising results in assessing concrete bridge decks over large spans. NDT can provide infrastructure owners with potential tools for decision-making and aid in diagnosing the extent of damage, flaws or deterioration within a member. Many different NDT methods can be used in detecting and visualizing the presence of internal imperfections or anomalies, yielding material properties and enabling the measurement of geometric characteristics of structural components. In this study, an approach is presented to expand the knowledge and to understand better the advantages and limitations of four NDT methods: Portable Seismic Property Analyzer (PSPA), Ultrasonic Tomography (MIRA), Ground Penetrating Radar (GPR), and Electrical Resistivity for the detection of delamination in concrete bridge decks with aging. The outcome of this research study is useful for researchers in transportation infrastructure agencies to differentiate between different types of defects, to estimate the location and size of the defects from information obtained by different NDT methods, and for decision-making on existing transportation infrastructures. From the results presented in this study, the MIRA technology turned out to be the most promising tool.

Table of Contents

List of Tables

List of Figures

Chapter 1: Introduction

1.1 Problem Statement

Delamination within concrete bridge decks occurs due to water and deicing salts penetrating the concrete; resulting in the corrosion of reinforcing steel. Consequently, a fracture parallel to the surface of the concrete structure is often induced at the top of the reinforcement layer; due to the corroded rebar. The delamination is then subjected to expansion over a large span; risking the overall stability of the structural element. It is therefore necessary to monitor the condition of the concrete structures and gain an in-depth understanding of the extent of deterioration the structure is enduring.

Several researchers have been involved in studying the accuracy, precision, ease of use, and cost of different NDT methods (Wimsatt et al., 2012; Gucunski et al., 2013). This thesis proposes an approach to expand the knowledge and to better understand the advantages and limitations of different NDT methods for the detection of delamination in concrete bridge decks with aging. For this purpose, a specimen built at The University of Texas at El Paso (UTEP) was tested utilizing various NDT tools, such as the Portable Seismic Property Analyzer, Ultrasonic Tomography (MIRA), Ground Penetrating Radar and Resistivity.

1.2 Organization of Thesis

This thesis is organized in six chapters. The current introductory chapter describes the problem statement of existing transportation infrastructures and the primary objective of this thesis. Chapter 2 presents a literature review of different NDT methods for testing concrete infrastructure. Each method is introduced and a brief summary of each method is provided. Chapter 3 summarizes the process of the experimental investigation and data collection during the

implementation of NDT testing in the concrete specimen. Chapter 4 presents the experimental investigation performed and a detailed summary of activities. Chapter 5 describes detailed test results obtained by each NDT tool. Chapter 6 contains a summary of the thesis, conclusions and recommendations for future work.

Chapter 2: Literature Review

2.1 INTRODUCTION

This chapter begins with an introduction of the effects that deterioration in delaminated areas of concrete bridge decks cause. The final section briefly discusses some of the NDT methods used for thickness measurement, flaw detection and material characterization.

2.2 DELAMINATION IN CONCRETE BRIDGE DECKS

The overall service life of concrete structures can be severely affected by delamination. It is essential to monitor and maintain these structures at early ages so repairs can be made before large-scale deterioration occurs (Azari, 2012). Corrosion-induced delamination manifests as cracking planes that are formed when reinforcing steel corrodes. The dominant deterioration mechanism is the chloride-ion induced corrosion of reinforcing steel (Weyers et al., 1993). The delamination is generally created above the reinforcing steel layer parallel to the surface (usually 50 mm to 150 mm below the surface). Delamination may extend over a substantial area. The delamination can propagate to the surface, causing large areas of spalling and affecting the overall integrity of the structure (Maser and Roddis, 1990; Washer et al., 2009).

2.3 NDT METHODS FOR CONCRETE STRUCTURES

According to the studies presented in SHRP2 Projects R06A (Gucunski et al., 2013) and R06G (Wimsatt et al., 2012), the most promising NDT methods for the evaluation of concrete bridge decks and tunnel linings are the ground penetrating radar, impulse response, infrared thermography, and seismic methods. For the detection of delamination, voids, and cracks within structures, the impact echo and ultrasonic surface wave methods have shown promising results (Gucunski et al., 2000; Yuan and Nazarian. 2000). Furthermore, the ultrasonic tomography has shown to be an efficient method in pavement thickness measurement (Vancura et al., 2013), joint

deterioration measurements, cracking in concrete, debonding and delamination in concrete (Wimsatt et al., 2012). The electrical resistivity method has showed promising results in pinpointing areas with high corrosive environments and areas where the environment does not facilitate corrosion (Gucunski et al., 2013). This work expands further investigation of these technologies. The principles of the NDT methods used for this work are presented below.

2.4 PORTABLE SEISMIC PROPERTY ANALYZER (PSPA)

The portable seismic property analyzer (PSPA) allows the determination of various properties and defects by monitoring the propagation of stress waves in the medium. Two wave propagation techniques, i.e., the ultrasonic surface wave (USW) and impact echo (IE), can be carried out with the PSPA.

Figure 2.1 shows a typical PSPA unit consisting of an electronic box, a source and two high-frequency receivers. A portable computer is connected to the electronic box for data acquisition. Depending on the type of evaluation being performed, the source-receiver spacing configuration can be modified by the user.

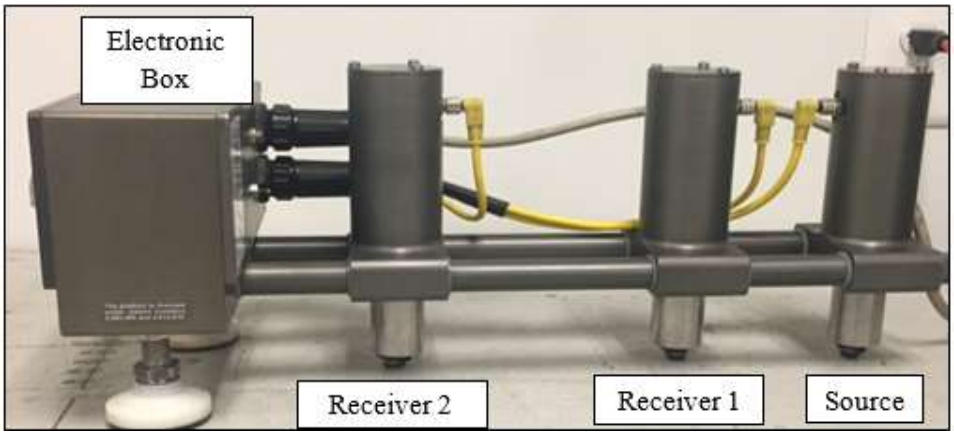

Figure 2.1 – Portable Seismic Property Analyzer (PSPA)

The USW method is applied to determine the average surface wave velocity by obtaining time records from the two receivers. Given that modulus the elastic (E) of the material is a function of the surface velocity (V_{ph}), Poisson's ratio (ν), and the mass density (ρ), the elastic modulus can be determined from Equation 2.1:

$$E = 2\rho(1-\nu)[1.13-0.16V_{ph}]^2 \tag{2.1}$$

Simultaneously, the near receiver's time record can be used to determine the thickness of the medium or to obtain the depth to a defect inside the material with the IE method. The IE analysis method consists of filtering the record to minimize the surface wave energy and conducting a fast-Fourier transform so that the return frequency can be calculated. Since the thickness (h) is a function of compression wave velocity (V_p), return frequency (f), and shape factor (α), then the thickness of the medium can be estimated through Equation 2.2:

$$h = \frac{\alpha V_p}{2f} \tag{2.2}$$

2.5 ULTRASONIC TOMOGRAPHY (MIRA)

An ultrasonic tomographer known as the MIRA (Figure 2.2), allows for the determination of various properties of a concrete including the thickness, detection of delamination and debonding, and determination of the depth and location to reinforcement. The MIRA system is based on the ultrasonic pitch-catch method, where the ultrasonic energy is transmitted at a certain angle to the surface of the material, and received as reflected energy returning at the reflected angle. The device consists of an array of dry point contact (DPC) transducers arranged into 12 blocks, each block possessing 4 transducers. The transducers emit shear waves into the material.

The transducers impact the surface, providing wave front penetration that diagnose the concrete structure up to a depth of 3 ft. The transducer array permits many pitch-catch, time-of-flight measurements to be made in a short period of time. The onboard computer controls which block of transducers acts as the transmitters, while the remaining blocks act as receivers. Figure 2.3 shows the multiple ray paths involved during a test with MIRA. The array is processed within the system providing a 2-D image of the concrete cross section. The 2-D scans are then analyzed with appropriate software to reconstruct a 3-D image of the structure, including B-scans, C-scans and D-scans of the structure (see Figure 2.4) (Popovics et al., 2017).

Figure 2.2 – MIRA Device (transducers shown)

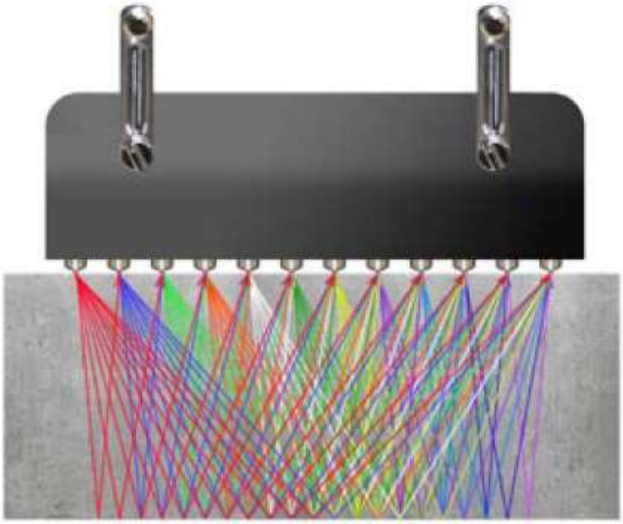

Figure 2.3 – Multiple ray paths involved during MIRA testing

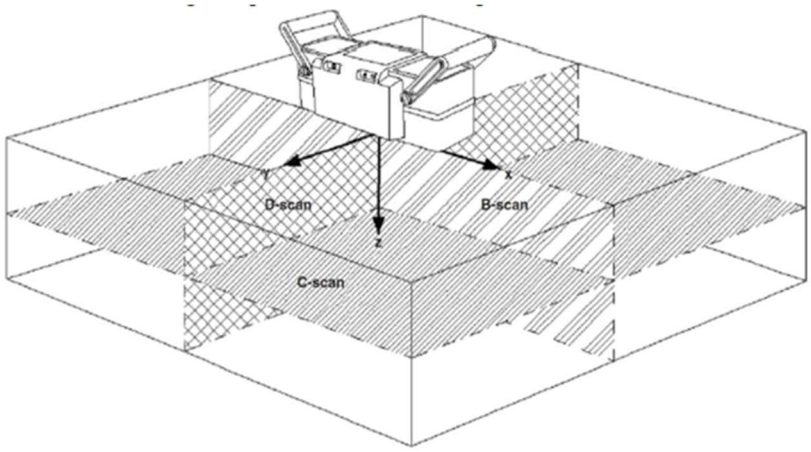

Figure 2.4 – B-scan, C- scan, D-scan (White et al., 2013)

2.6 GROUND PENETRATING RADAR (GPR)

The Ground Penetrating Radar (GPR) is a NDT technique that is based on the principle of sending short pulses of low-level electromagnetic (EM) energy into the material. Simultaneously, the GPR system measures the effects that the material has on the reflection of the transmitted pulse. From the received reflections, the layer boundaries can be deduced, and various characteristics and assumptions can be formulated about the material. Often utilized to obtain layer thickness, the GPR measures this by sending a pulse into the material and measuring the travel time between the reflection at the top of the pavement and the reflection at the bottom of the pavement (Romero and Roberts, 2002). A typical ground-coupled GPR device setup is displayed in Figure 2.5.

Figure 2.5 – Ground Penetrating Radar (GPR)

2.7 ELECTRICAL RESISTIVITY

The resistivity measurements were carried out using a Wenner configuration (see Figure 2.6). In the Wenner configuration, the electrode layout consists of equally spaced four probes are coupled to the concrete surface to measure the electrical resistivity in concrete. Electrical resistivity is used for moisture detection that may be penetrating the concrete through cracks. Cracked areas open pathways for chlorides to travel to the location of the reinforcement points; initiating the corrosion process. The higher the electrical resistivity of the concrete, the lower the current passing from the anodic and cathodic areas of the reinforcement will be. Table 2.1 displays typical indicators of corrosion rate given the resistivity.

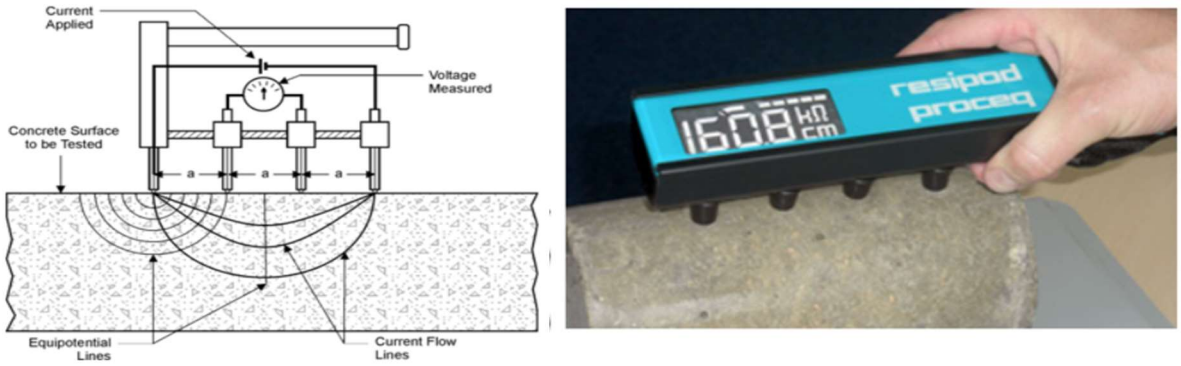

Figure 2.6 – Resistivity Testing Schematic and Device (Gowers and Millard., 1999)

Table 2.1 – Corrosion State of Reinforced Concrete given Resistivity (Gowers and Millard., 1999)

Resistivity (kΩ x cm)	**Corrosion Rate**
< 5	Very High
5-10	High
10-20	Moderate-low
> 20	Low

Chapter 3: Data Collection

This chapter summarizes the procedures employed by the different methods to collect NDT data. A detailed description of the data processing and interpretation of each method used to analyze the concrete specimen is presented.

3.1 PSPA Data Collection Process

PSPA data collection consists of four to six continuous impacts from the hammer that produce three output time records. The first set of impacts is performed to adjust the device settings, while the last three output time records are saved for further data analysis. The time record in Figure 3.1 represents the highly attenuated response of the source, while the other records correspond to the output from Receiver 1 and Receiver 2. The responses from the first receiver are used for the impact-echo (IE) analysis. This analysis primarily consists of filtering the record to minimize the surface wave energy and conducting a fast-Fourier transform so that the return frequency in Equation 2.2 can be estimated.

The records from Receiver 1 and Receiver 2 are used for the USW analysis. The two time records are subjected to spectral analysis to develop a phase spectrum representing the time-delay between the two receivers. For demonstration, a phase spectrum is displayed in Figure 3.1. The phase spectrum is used to calculate the dispersion curve, i.e., the variation of velocity with wavelength. Finally, the dispersion curve is averaged to obtain the elastic modulus of the material.

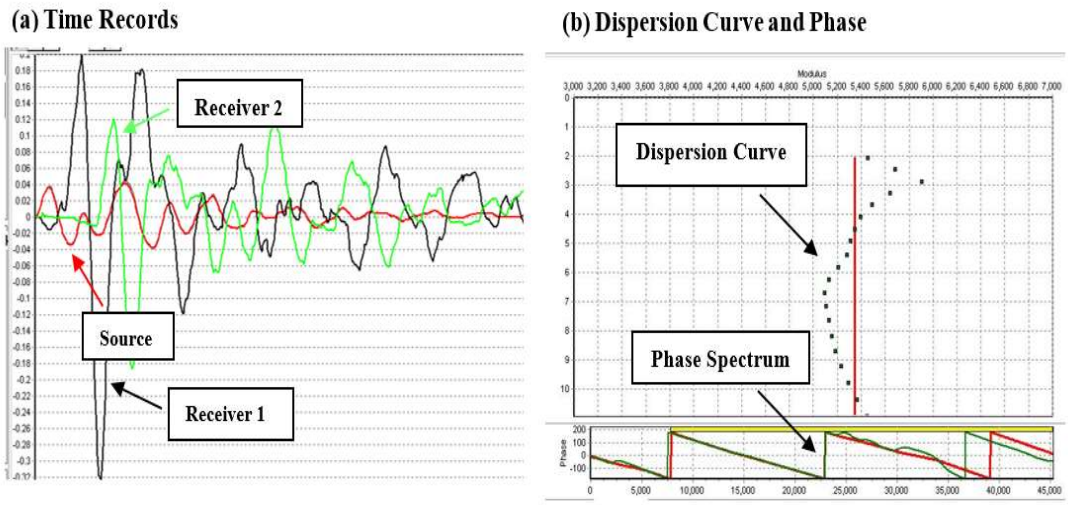

Figure 3.1 – PSPA Data Reduction and Results

3.2 ULTRASONIC TOMOGRAPHY (MIRA) DATA COLLECTION PROCESS

The ultrasonic pulse-echo method uses transmitting and receiving transducers through a pitch-catch method. One of the transducers sends out a stress-wave pulse while another transducer receives the reflected pulse. The travel time from the initiation of the pulse to the arrival of the echo is measured (Δt). The wave speed can then be computed, enabling the depth of the reflecting interface to be determined. With the shear wave velocity (C_s), the depth of the member (d) can be calculated from Equation 3.1:

$$d = Cs\,\frac{\Delta t}{2} \tag{3.1}$$

Figure 3.2 depicts reflections on interfaces, which could be the result of reflection against a back wall, reinforcement bars, or internal concrete-air interfaces (e.g., voids, cracks and delamination). The presence of these interfaces results in stronger reflections.

Data collection is performed by establishing a symmetrical scanning grid in the area of interest. The grid is composed of horizontal steps; referring to the distance between the scan lines. The perpendicular distance to the scan lines is termed the vertical step.

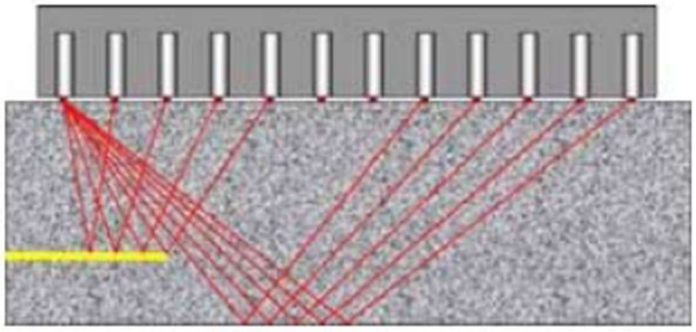

Figure 3.2 – MIRA Reflections Scan over Material

3.3 GROUND PENETRATING RADAR (GPR) DATA COLLECTION PROCESS

A GPR antenna sends high-frequency EM waves into the material. The presence of rebar, or other obstructions or interfaces, will cause a portion of the energy to reflect to the surface and be received by the antenna. The remainder of the energy continues to travel beneath this reflector. Additional energy reflects to the receiver from other reflectors until the EM wave dissipates. The electrical conductivity and relative dielectric permittivity impact the signal response caused by variations in these electrical properties. The ability of GPR energy to penetrate the medium and the speed at which GPR propagates through medium are dependent on these properties.

Data collection is performed by defining a scanning grid for the GPR system to acquire linescans as shown in Figure 3.3. The GPR system is scanned over a defined grid to yield a 3-D representation of the concrete profile. In the 3D model of the structure, the shallow delaminated areas are clearly distinguished, while deep delaminated areas are not as clearly distinguished due to the obstructions or interfaces that cause a portion of the energy to reflect to the surface.

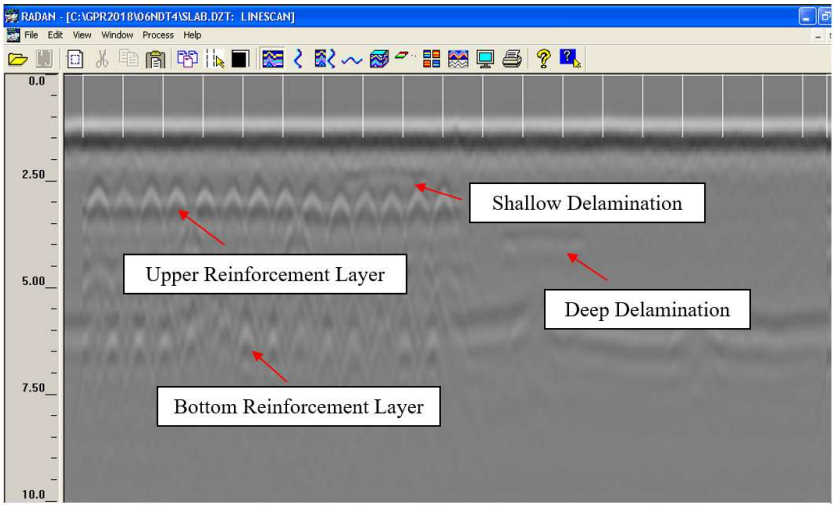

Figure 3.3 – GPR Line Scan from SIR 20 software

3.4 ELECTRICAL RESISTIVITY DATA COLLECTION PROCESS

The Wenner Probe works on the principle of applying a current between the outer electrodes; having the two inner electrodes measure the potential of the electric field. Since resistivity (ρ) is a function of electrode separation (a), voltage (V), and current (I), resistivity can be calculated as shown in Equation 3.2:

$$\rho = \frac{2\pi aV}{I} \tag{3.2}$$

Data collection is performed by first establishing a grid pattern over the area of interest. The probe is then placed and pressed over a wet surface at each test location. Each probe reading is then observed and recorded. The presence of reinforcement can influence the readings; therefore, it is recommended for the probe to set in specific orientations as shown in Figure 3.4. Location "A", represents the best position to set the probe, where reinforcement is not present underneath. Locations "B", "C", and "D" represent good, fair and poor locations to set the probe, where the contact of the probes with the location of the reinforcement is denser.

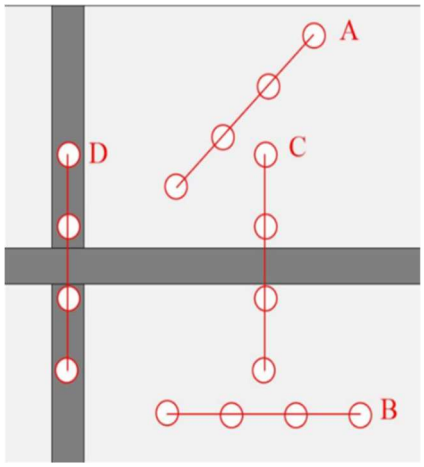

Figure 3.4 – Wenner Probe Placement Orientation Given Existing Reinforcement

Chapter 4: Experimental Investigation

4.1 INTRODUCTION

The purpose of this task was to collect baseline data from the different NDT methods and evaluate advantages and limitations of these methods for the detection of delamination in concrete bridge decks with aging. The methods were applied to a reinforced slab emulating a bridge deck based on TxDOT standards. Data were collected regularly with each device over a 28-day span and then monitored thereafter in three-month intervals.

4.2 SPECIMEN

Figure 4.1 shows the construction images of the deck. A 20-ft long x 8-ft wide x 8-in. thick concrete deck was constructed at UTEP. The slab, which was constructed outdoors in an arid-desert climate, was not exposed to precipitation or direct sun. The slab was constructed in the winter under an air temperature of about 50°F.

Figure 4.2 details the plan and cross sections of the reinforcement layers. The single bridge deck was constructed to represent two separate experimental regions. Region I represents a slab with two layers of reinforcement, while Region II represents an unreinforced slab.

Eight artificially delaminated areas of various sizes and depths were simulated using 3-mm thick cardboard material lined with thin plastic. Four larger delaminated areas of 2-ft x 2-ft were incorporated, along with another four smaller delamination areas of 1ft x 1ft. The precise location of the delaminated areas, along with the predefined testing grid used for all testing experiments are shown in Figure 4.3. The vertical and horizontal spacing of the testing grid was 8-in.

The concrete mix design provided by Jobe Materials is shown in Table 4.1. As shown in Table 4.2, three sets of 6 in. by 12 in. specimens were utilized to obtain the 1, 3, 7 and 28-day compressive strengths and moduli. "Naturally Cured" specimens were left at the location of the slab, while "Standard Cured" 1 and 2 were placed in an environmental chamber to be cured under standard curing conditions (70°F and 100% humidity). The naturally cured specimen, in comparison to the standard cured specimens, yielded lower elastic moduli and compressive strengths due to different temperature and humidity conditions. The standard cured specimens presented similar elastic moduli and compressive strengths, with both properties increasing with time (signifying the hardening of the concrete).

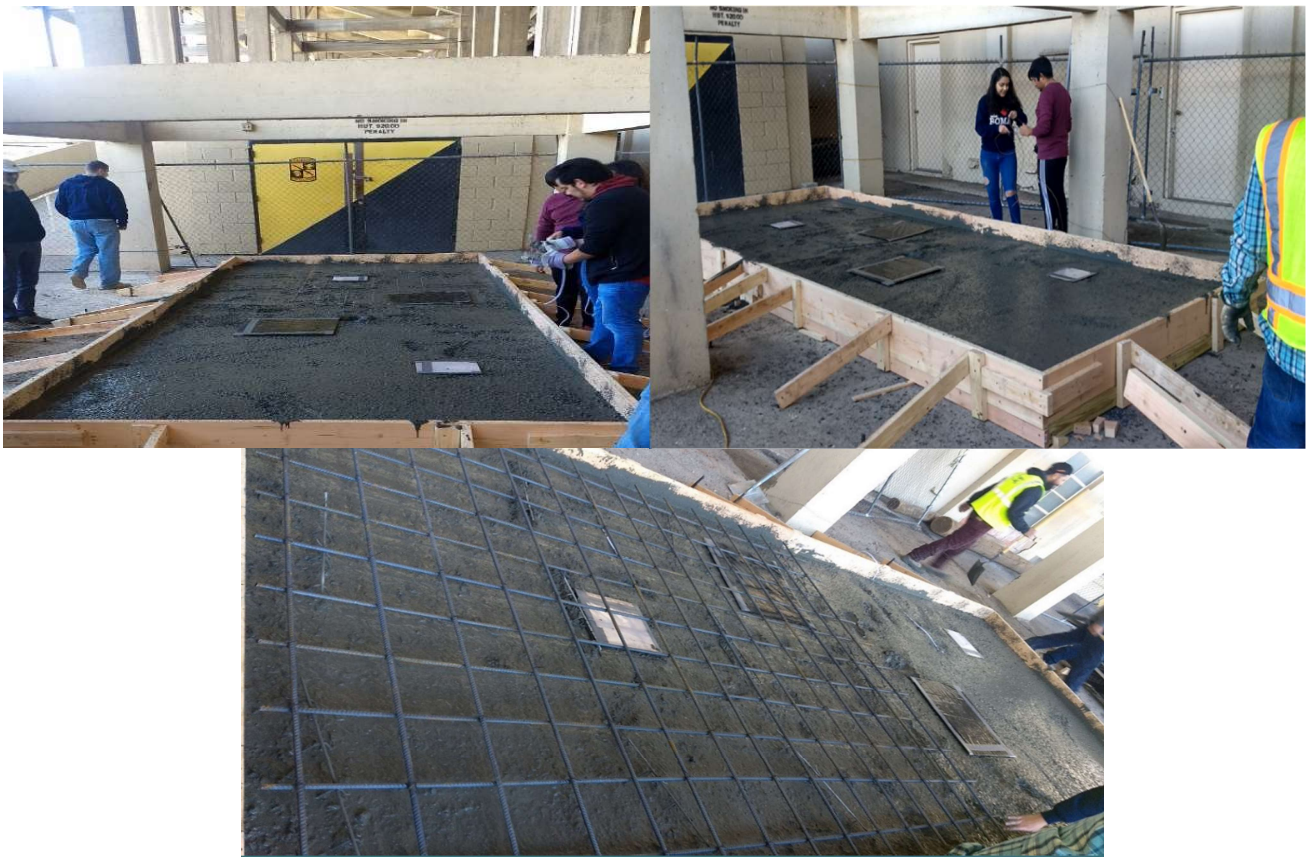

Figure 4.1 – Constructed Concrete Deck with Simulated Delamination Areas

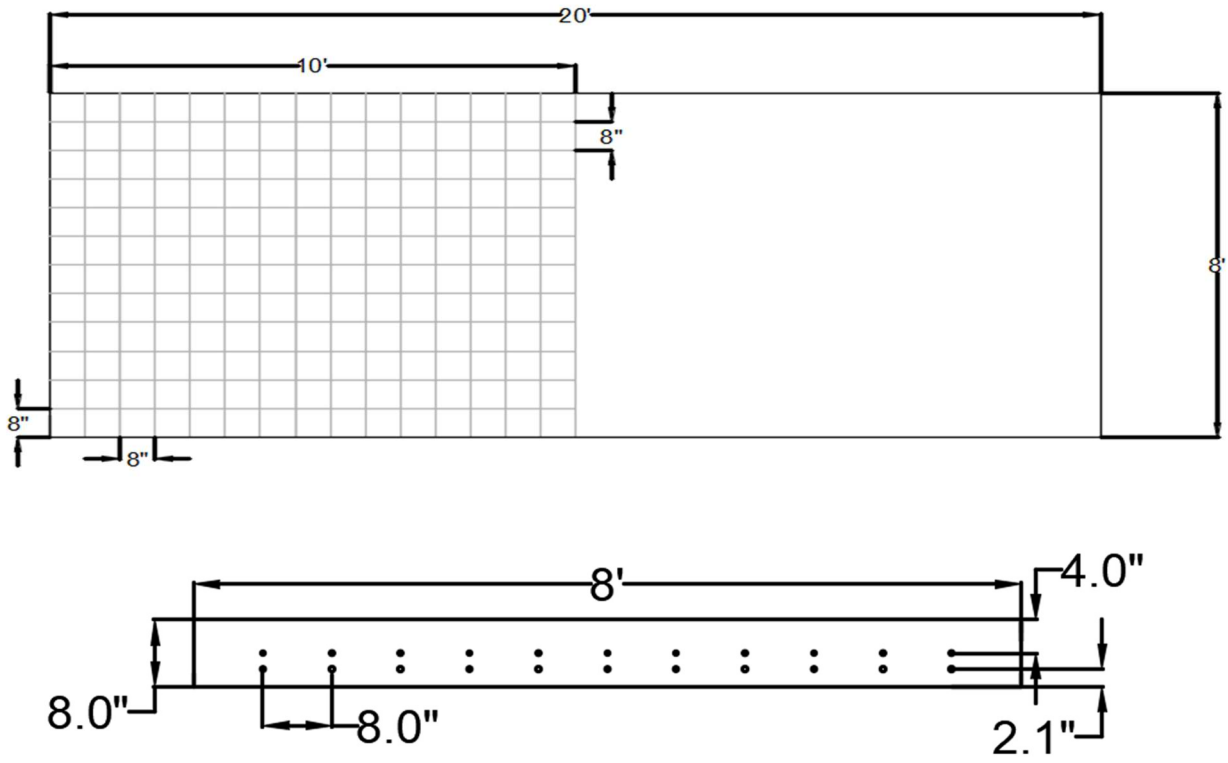

Cross Section of Longitudinal Reinforcement

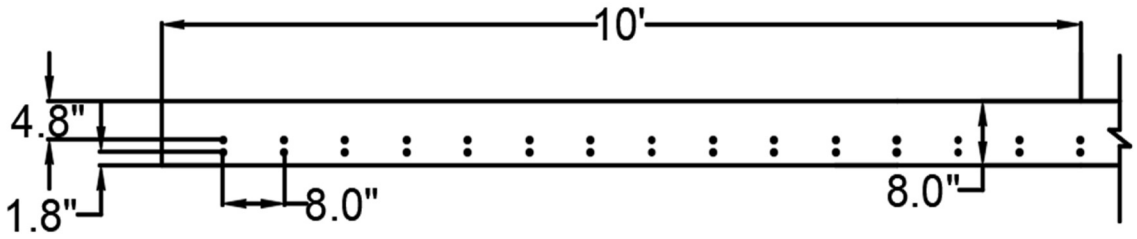

Cross Section of Transverse Reinforcement

Figure 4.2 – Cross Section Areas of Reinforcement Layers

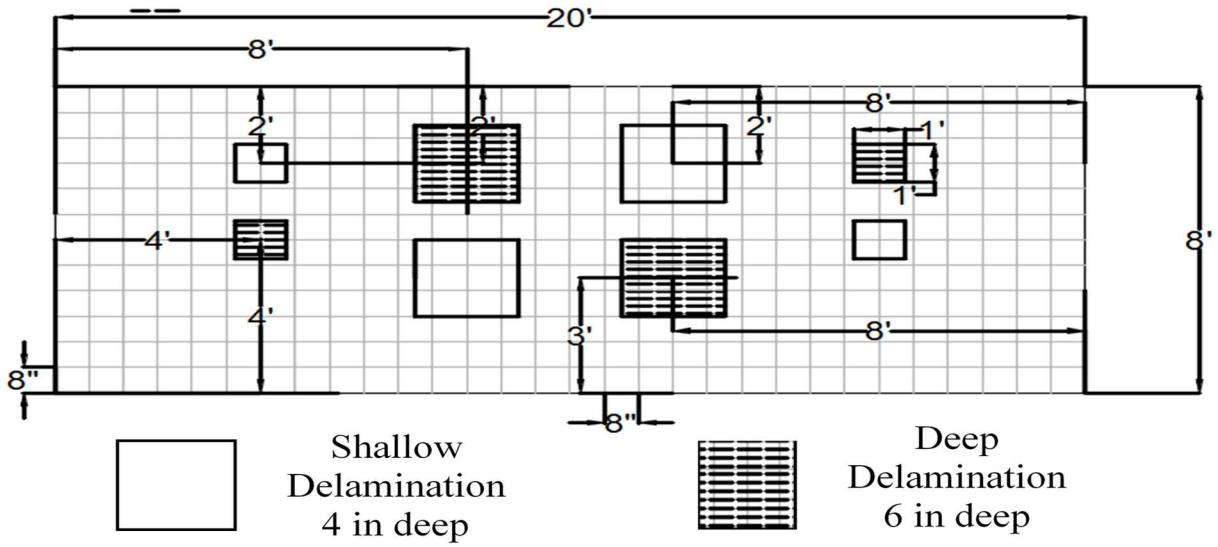

Figure 4.3 – Planar View of Delamination in Concrete Deck

Table 4.1 – Concrete Mix Design

Material	Design Quantity (lb)	Required (lb)	Batched (lb)	% Moisture	Actual Water (gal)
Sand	1240	7765	7720	4.4%	38.8
#67	1350	8185	8140	1.1%	10.1
#57	320	1933	1900	0.7%	1.5
3/6”	250	1502	1520	0.1%	
CEMENT	451	2706	2700	-	
FLYASH	113	678	670	-	
WATER	30.5	120	120	-	120.0
X-15A	23	138	130	-	
X-15B	23	138	140	-	
D8	5	30	30	-	

Table 4.2 – Modulus and Compressive Strength of Concrete

Naturally Cured 1			Standard Cured 1			Standard Cured 2		
Day	Elastic Modulus (ksi)	Strength (psi)	Day	Elastic Modulus (ksi)	Strength (psi)	Day	Elastic Modulus (ksi)	Strength (psi)
1	2355	486	1	3601	1448	1	3605	1215
3	3550	1573	3	4624	2874	3	4698	2703
7	4143	2673	7	4988	3527	7	5017	3051
28	5498	4167	28	6081	5118	28	6151	4556

Chapter 5: Data Analysis

5.1 Introduction

This chapter discusses the data analysis and results of each NDT tool used during the testing period on the concrete specimen. The data from each specific test day for each NDT test is presented as a contour map showing the variation of each quantity over the concrete slab.

5.2 Ultrasonic Surface Wave

The USW testing was performed 1, 5, 7, 12, 15, 112, 200 and 260 days post-pouring. For this NDT method, the testing was performed with a 16-in. spacing grid instead of the typical 8-in. grid, decreasing the number of test points. The variations in concrete modulus with time for regions 1 and 2 are shown in Figure 5.1. The error bars correspond to ±1 standard deviation (excluding the areas of delamination). The moduli from the two regions are quite similar indicating that the inclusion of rebar does not impact the measurements by USW method. Since the diameter of the rebar is small relative to the surface wavelength, the presence of steel reinforcement does not influence the propagation of the surface waves. Initially the modulus of the slab increased quite rapidly. After 28 days, the increase in modulus is rather small.

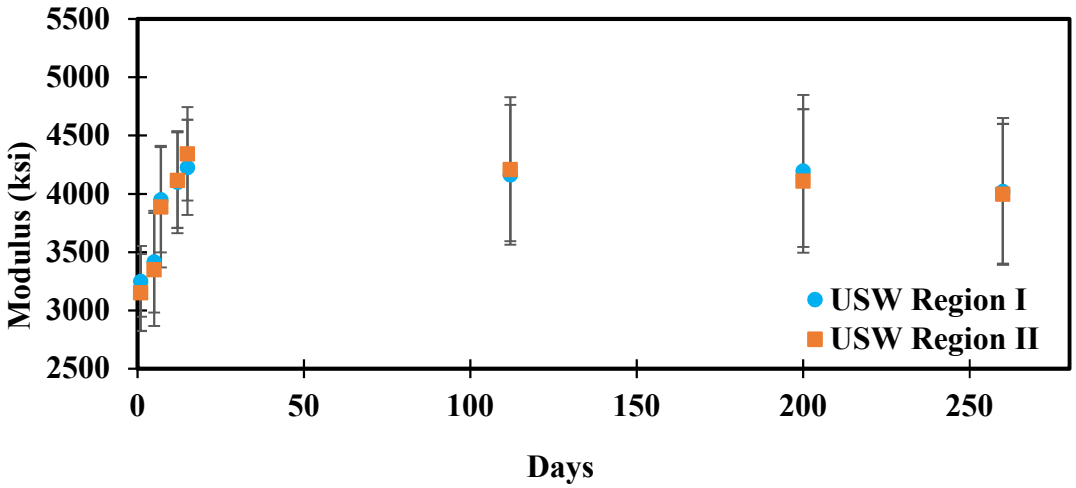

Figure 5.1 – Average Modulus through USW in Non-Delaminated Areas

The contour plots of average moduli at different ages are shown in Figure 5.2. For both, USW and IE contours, the dashed squares signify the location of the deep delaminated areas while the solid lines present the location of the shallow delaminated areas. Linear interpolation was used to contour the data, where the interpolated value at a query point is based on linear interpolation of the values at neighboring grid points in each respective direction.

The Surface waves have the greatest amplitude, relative to compression and shear waves, and attenuate rapidly with depth below the surface (Miller and Pursey 1955, Woods 1968). The USW method shows promise in detecting the shallow delaminated areas. During the early days of the concrete specimen, the deep delaminated areas are detected by the USW method. As time progresses, however, the hardening of the concrete prohibits further propagation, and therefore the rapid attenuation of the surface waves with depth is evident.

To furtherly analyze the impact of the grid density of the results, the data collection on day 112 was performed using an 8-in. spacing between each test point. Figure 5.3 presents the data from Day 112 with 8-in. and 16-in. grids. The denser grid presents a more detailed result as the low modulus values at the location of the shallow defects are thoroughly pinpointed. However, the density of points does not directly impact the overall results. In both schemes, the shallow defects are clearly observed in the contoured results.

5.3 IMPACT ECHO

The IE testing was performed 1, 5, 7, 12, 15, 112, 200, and 260 days post-pouring. For this NDT method, the testing was performed with a 16-in. spacing grid instead of the typical 8-in. grid, decreasing the number of test points. The variation in average return frequency (excluding the areas of delamination) from the reinforced and non-reinforced area obtained from each test day plotted with the error bars representing ±1 standard deviation with time is shown in Figure 5.4. A frequency peak of about 8 kHz dominates the response in the intact area, corresponding to the return frequency of the 8-in. slab in intact areas.

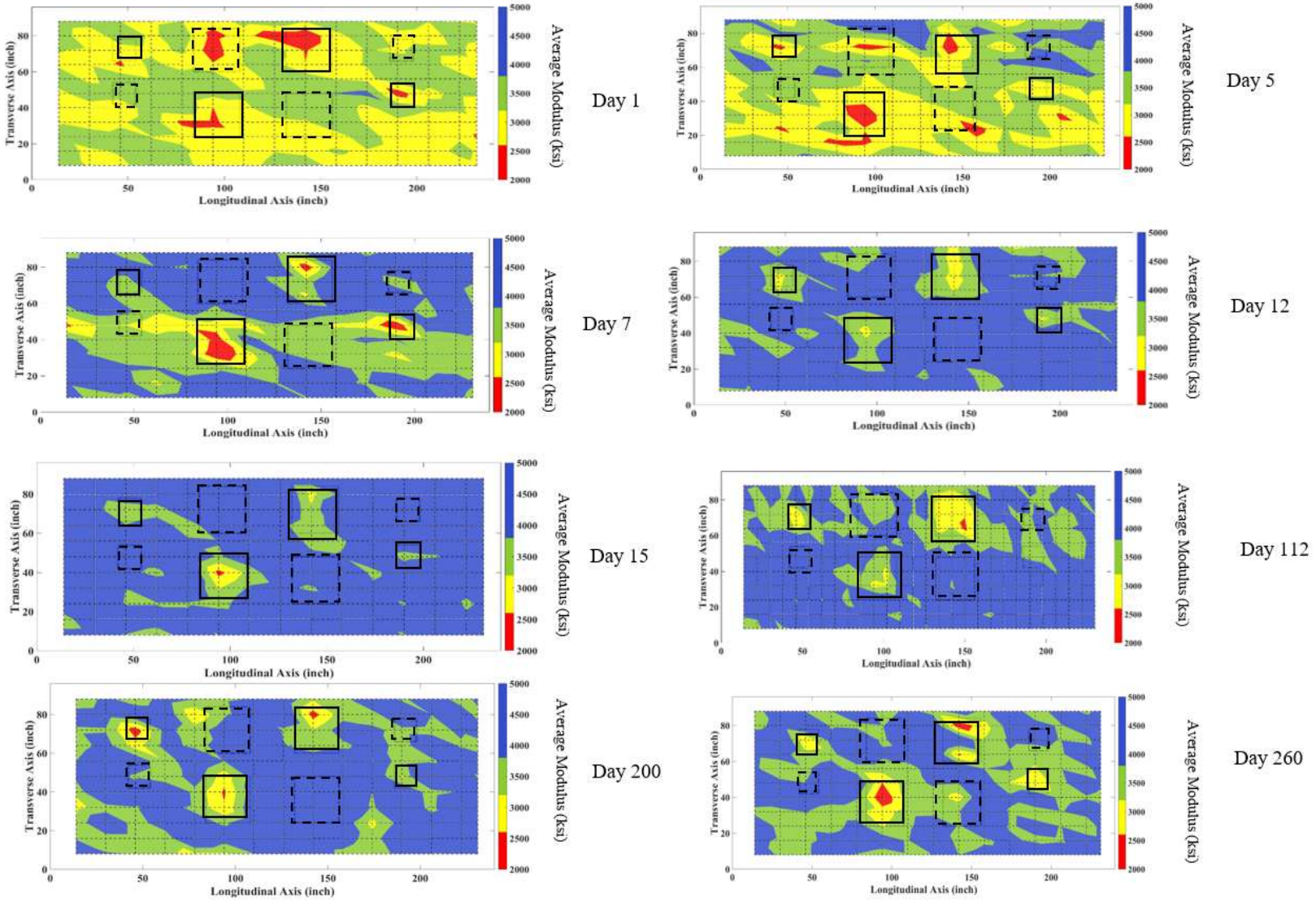

Figure 5.2 – USW Contour Maps of Modulus Variation in Non-Delaminated Areas

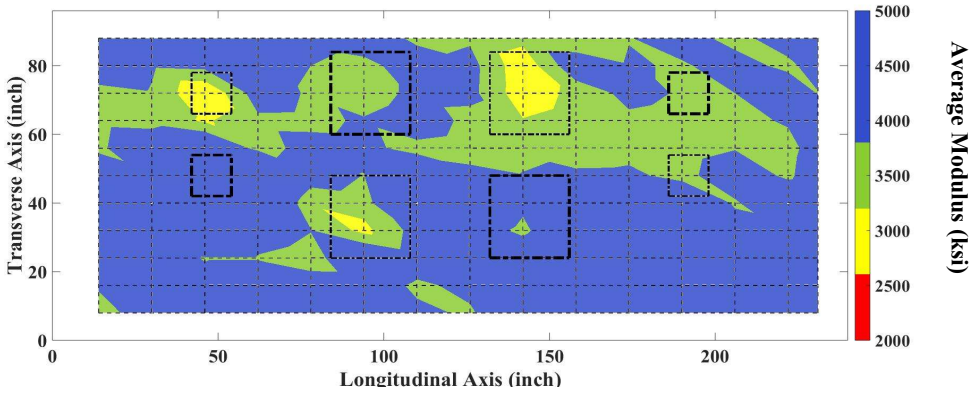

Day 112 – 8-in. Spacing Grid

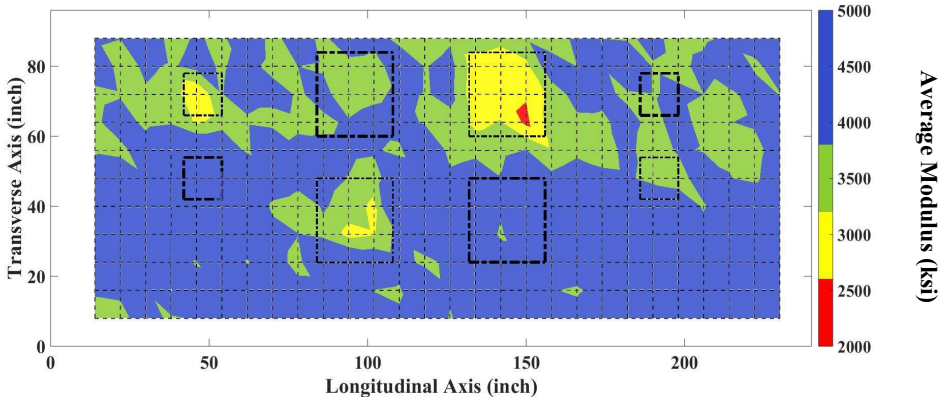

Day 112 – 16-in. spacing Grid

Figure 5.3 – USW Contour Maps of Modulus Variation with Different Testing Grid

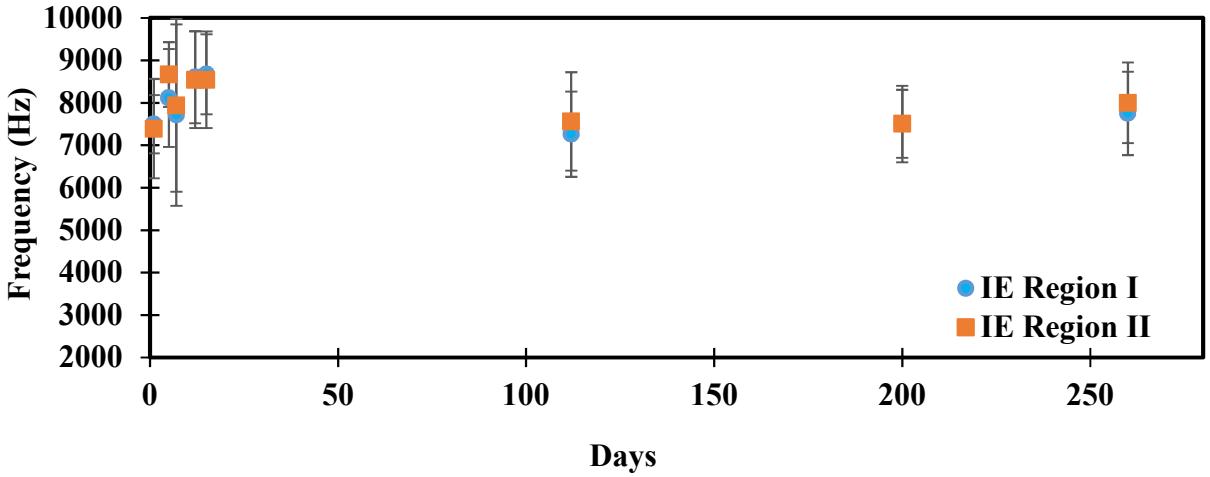

Figure 5.4 – Average Peak Frequency through IE in Non-Delaminated Areas

The contours of the IE return frequency for the slab at different times are shown in Figure 5.5. The flexural mode, with a peak frequency of around 3 kHz, is dominant for the shallow and deep delaminated areas. The IE method was able to detect the shallow and deep delaminated areas with 2-ft x 2-ft dimensions at all stages. There were a total of six frequency measurements at the location of each of these larger delaminated areas. These multiple test points allow the flexural mode of vibration to be evident at the location of these larger areas. The smaller delaminated areas (with 1-ft x 1-ft dimension) were not detected by the IE method at all stages due to only having one frequency measurement at the location of each of these defects. A denser grid may, therefore, provide better detection of these smaller areas. The smaller voids also don't reflect as much energy making them harder to detect. During the later days of the concrete specimen's life, the IE method, however, does not capture the defects as clearly, and the peak frequency seems to be disrupted. Though the reasons for this phenomenon are not exactly known, it might be attributed to the highly arid nature of El Paso (the concrete is bone dry).

As mentioned, the results from Day-112 were obtained from a denser data collection grid. Figure 5.6 presents the data from Day 112 with both (8-in. and 16-in.) grids. The denser grid presents a more detailed scheme at the location of the shallow and deep defects. However, the density of points does not directly impact the overall results. In both schemes, the peak frequency of 3 kHz at the location of most defects is evident.

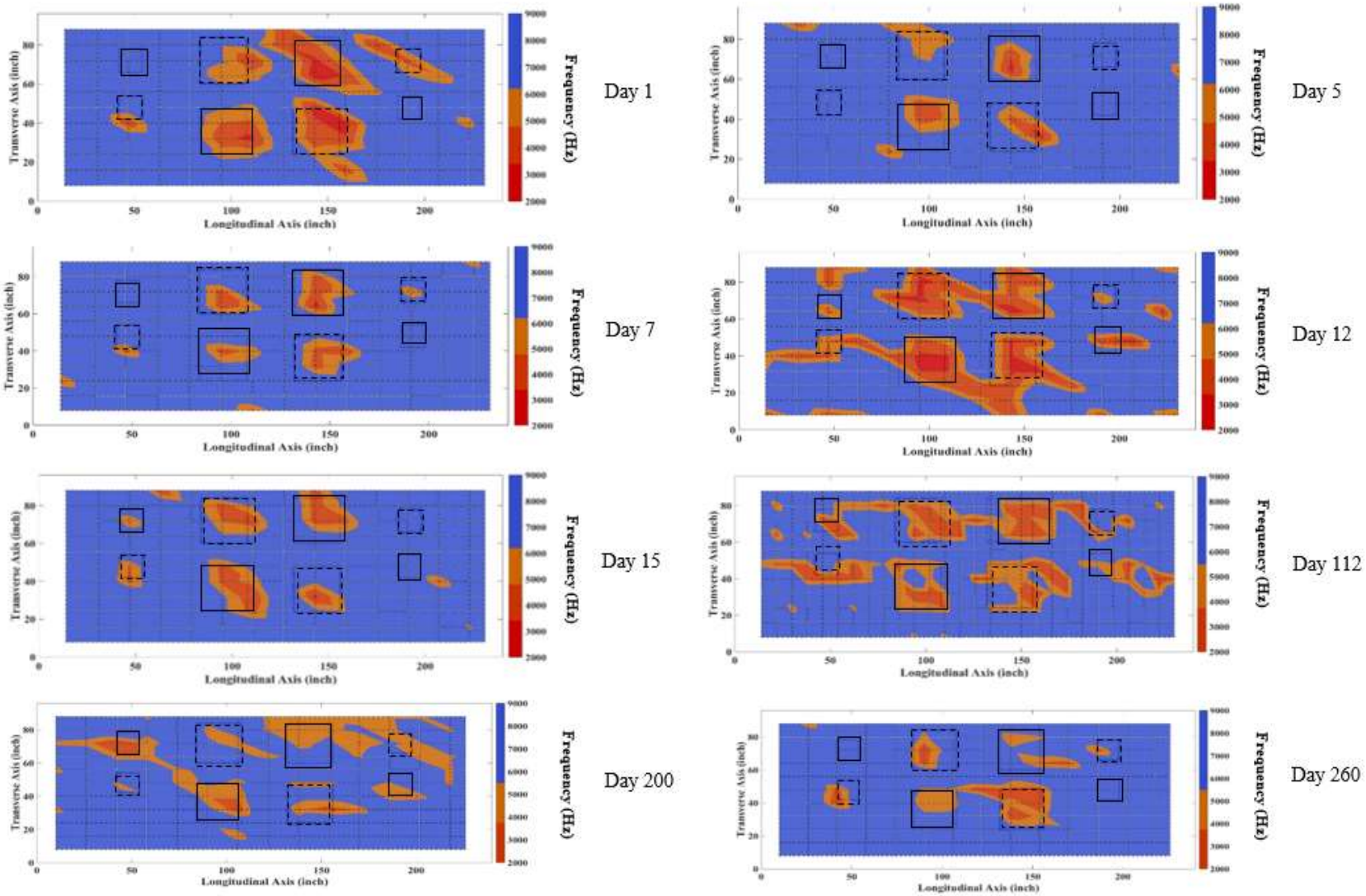

Figure 5.5 – IE Contour Maps of Peak Frequency

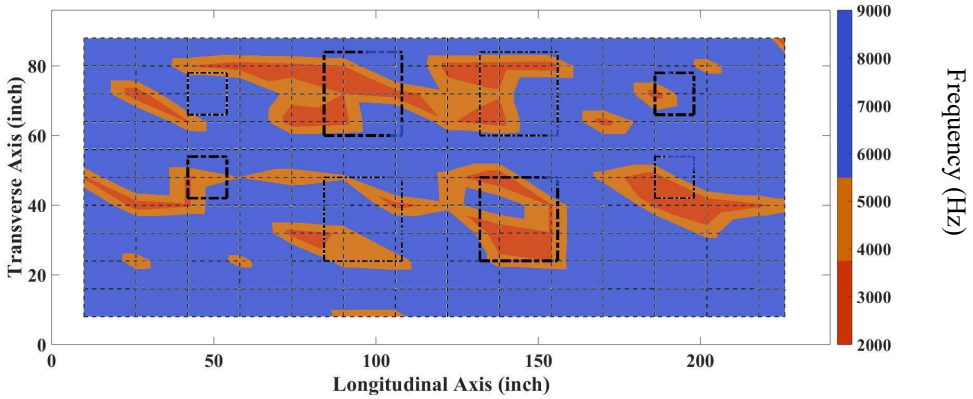

Day 112 – 8-in. Spacing Grid

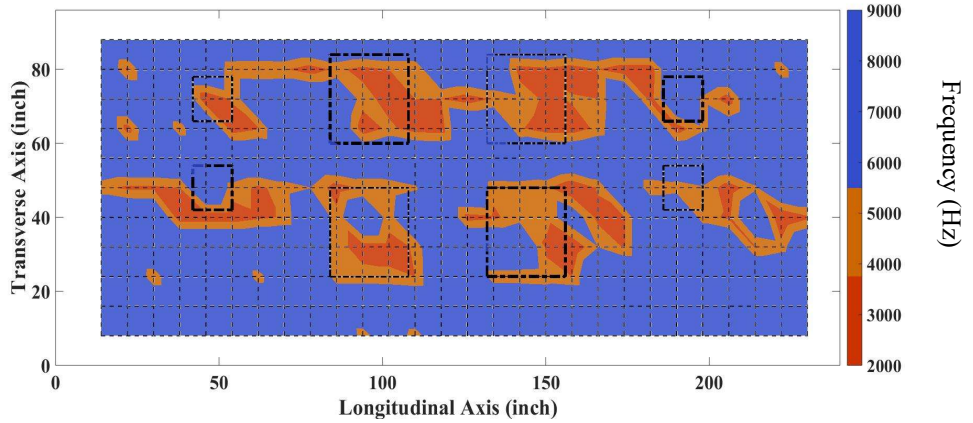

Day 112 – 16-in. Spacing Grid

Figure 5.6 – IE Contour Maps of Peak Frequency with Different Testing Grid

5.4 ULTRASONIC TOMOGRAPHY (MIRA)

The MIRA testing was performed 4, 8, 15, 20, 69, 158, 250 and 320 days after pouring. Figures 5.7 and 5.8 display C-scan cross sections of the volume at a depth of 4-in and 6-in., respectively. The dashed squares signify the location of the deep delaminated areas while the solid lines present the location of the shallow delaminated areas. These images present the reflection amplitude of the multiple array paths of the shear-wave transducers involved in MIRA testing. The Introview Concrete software (used to analyze MIRA data) has a threshold slider option, which allows all voxels for which the signal amplitude is lower than the selected threshold to not be

shown (as shown in the image's blank areas). When the slider option is left intact, the scans show reflection amplitude contouring thoroughly, as shown in the Appendix.

The MIRA captured all defects, including deep and shallow delaminated areas, as well as the reinforcement layers at each testing stage. The first reinforcement layer, however, is better contoured than the second reinforcement layer. This is due to the shear wave amplitude reflection disruption that the first layer of reinforcement causes, yielding contours that show a disturbed alignment of the deeper reinforcement layer. The delaminated areas, however, are clearly contoured for both shallow and deep defects.

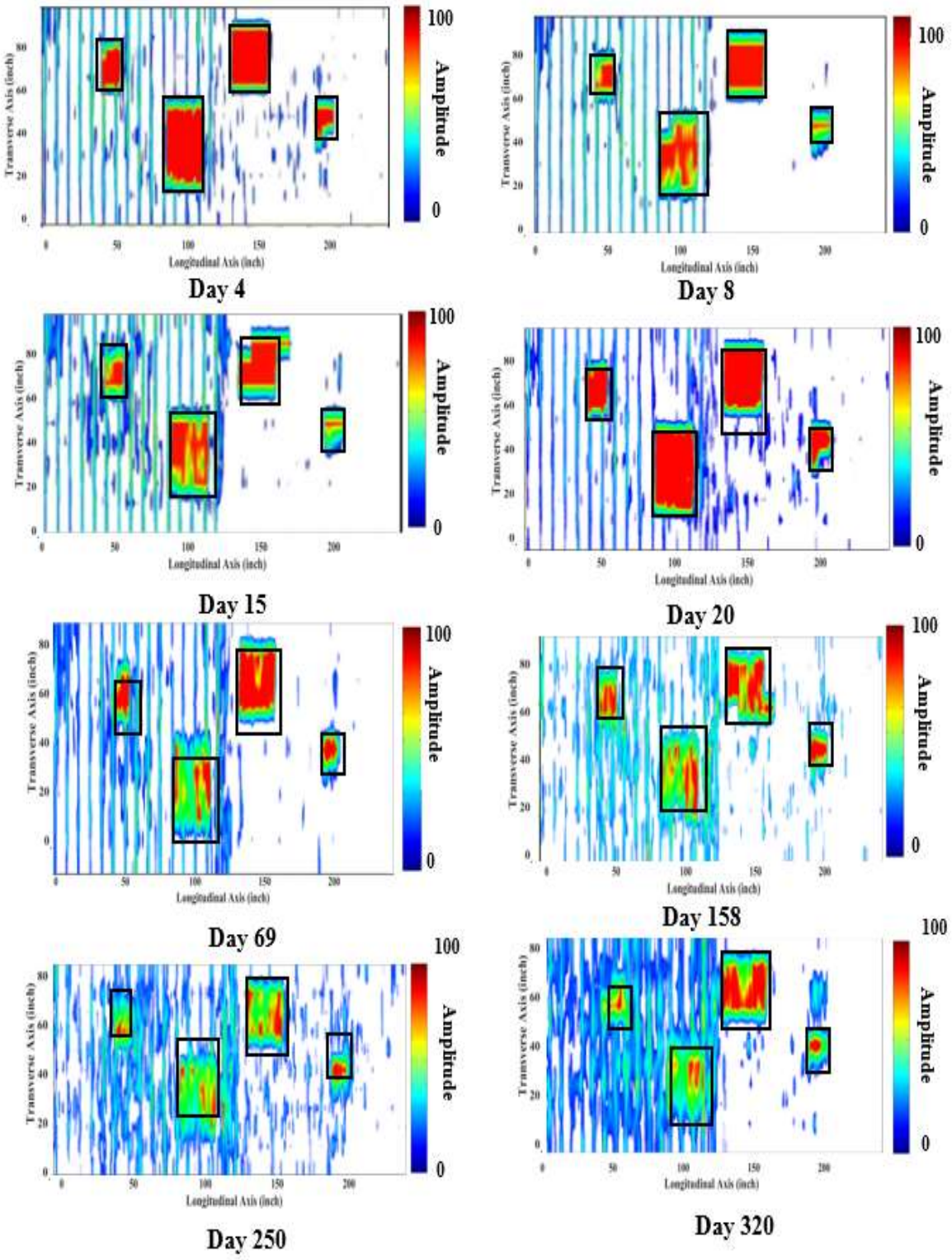

Figure 5.7 – MIRA 2D Shallow Delamination Contours at 4-in. deep

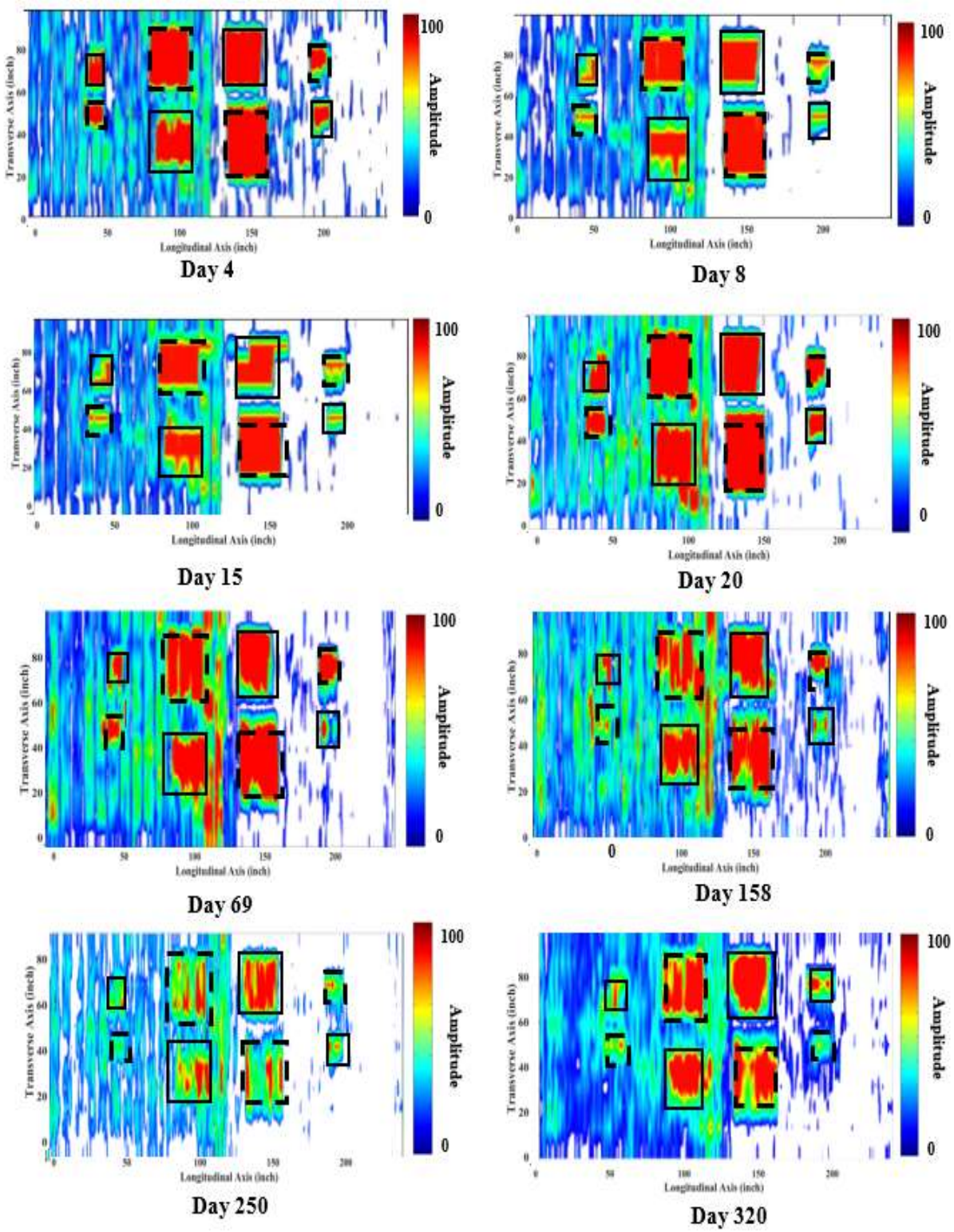

Figure 5.8 – MIRA 2D Shallow and Deep Delaminated Contours at 6-in. deep

5.5 GROUND PENETRATING RADAR (GPR)

The GPR testing was performed 20, 22, 108, 180, and 250 days after pouring. The average electromagnetic velocity (excluding the delaminated areas) from the reinforced and non-reinforced area obtained from each test day are plotted with the error bars representing ±1 standard deviation in Figure 5.9. RADAN software is used to analyze GPR data, where the user is able to select the different layers shown in the line scans; this generates an output file with the arrival time of the reflected pulses from the bottom of the slab. The electromagnetic velocity values were then calculated by dividing the thickness of the slab (8 in.) by the time record values (in nanosecond).

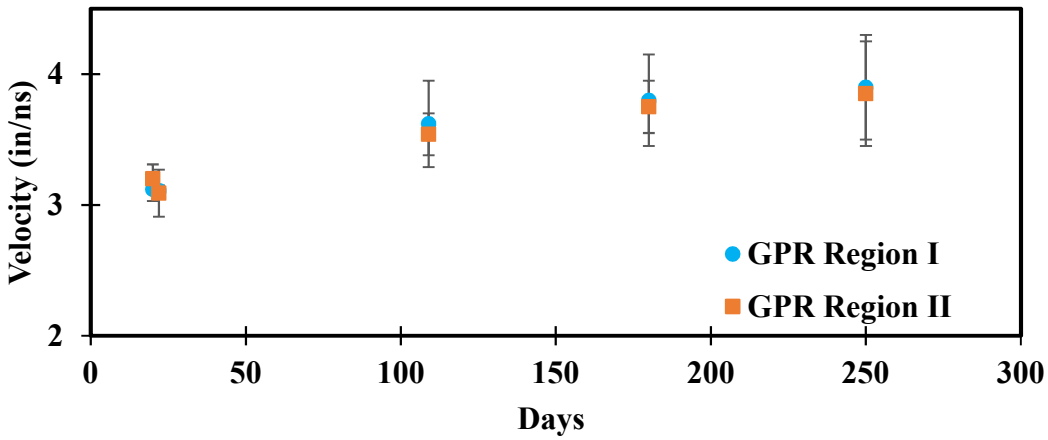

Figure 5.9 – Average Electromagnetic Velocity through GPR in Non-Delaminated Areas

The 3D GPR scans are shown in Figure 5.10 at different depths. Day 20 and 22 post-pouring indicate major anomalies in the electromagnetic wave amplitude reflection at the location of the shallow defects (shown in the red areas). However, during the later days of the specimen (Day 108 – 250) the reflections at the locations of the defects not as clearly shown. This can be due to the hardening of the concrete. As moisture is lost in the concrete, the dielectric constant of the concrete decreases, and its contrast with the plastic cardboard material also diminishes, causing less energy discrepancy between the two materials. Deep delaminated areas are not as clearly distinguished due to the obstructions or interfaces at the shallower areas of the concrete specimen

that cause a portion of the energy to be reflected back to the surface. Minor reflections indicating the anomalies in these deeper defective areas are shown at all concrete stages. The shallow layer of metal reinforcement presents a strong energy reflection from the electromagnetic waves at all stages of the concrete specimen (as shown by the red aligned reflections symbolizing the shallower rebar layout). The deeper reinforcement layer, however, is not as clearly captured due to the obstruction that the shallower reinforcement layer imposes, causing a strong portion of the energy to be reflected back to the surface.

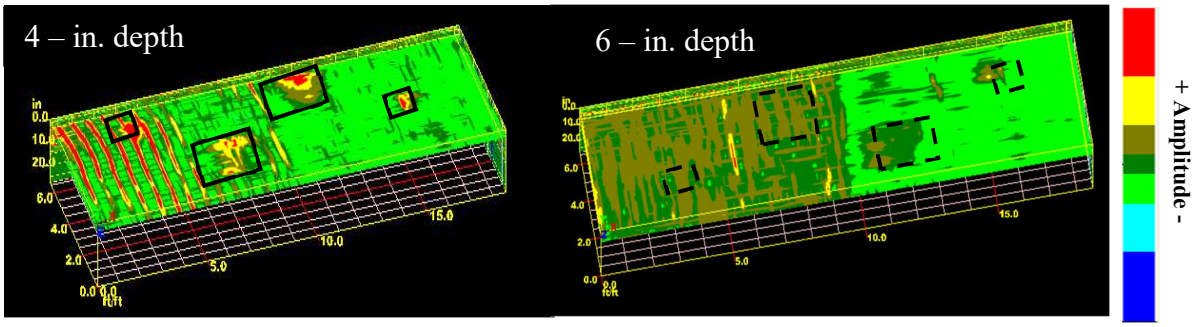

Day 20

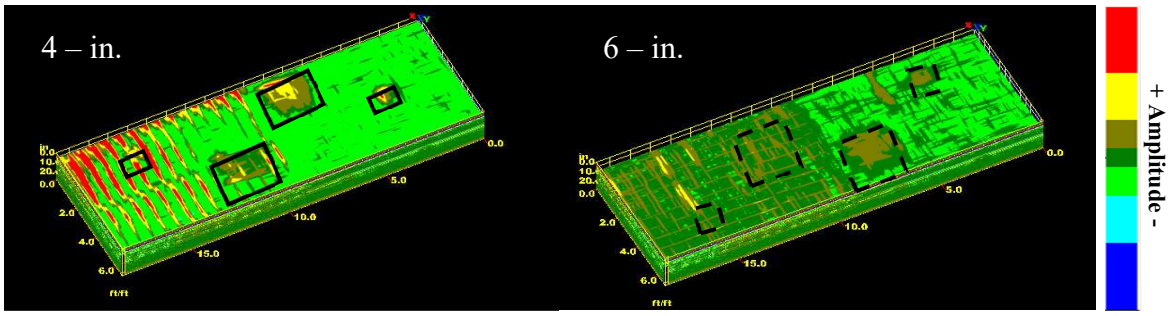

Day 22

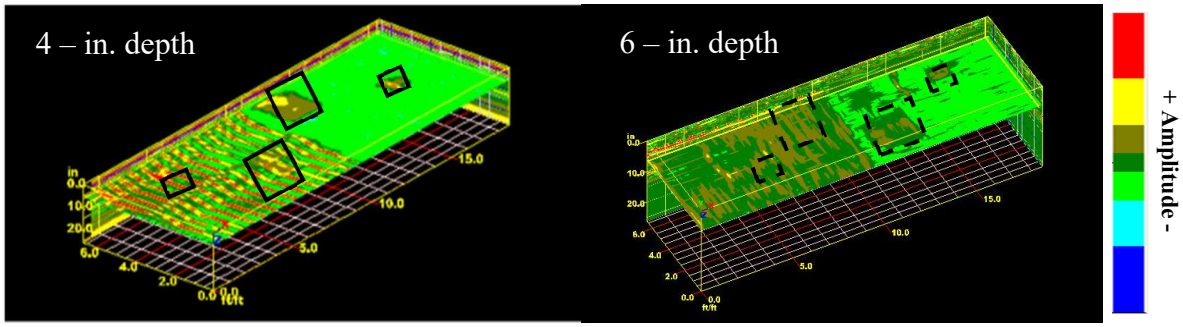

Day 108

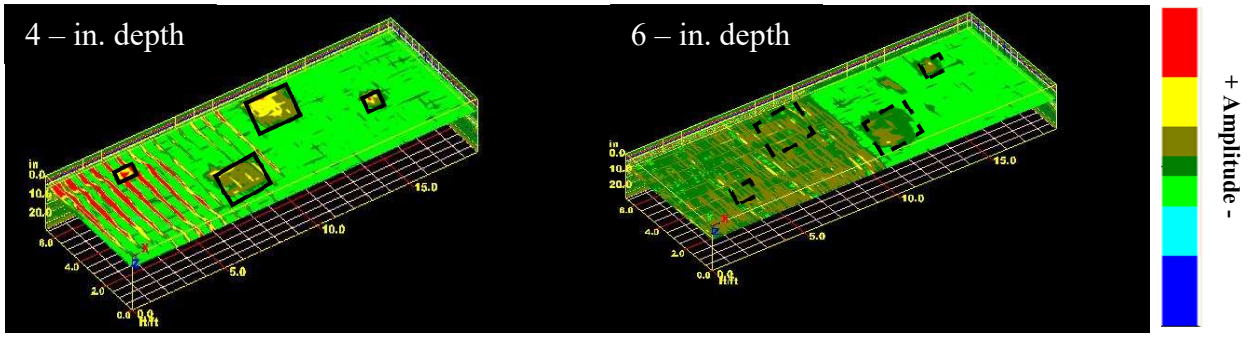

Day 180

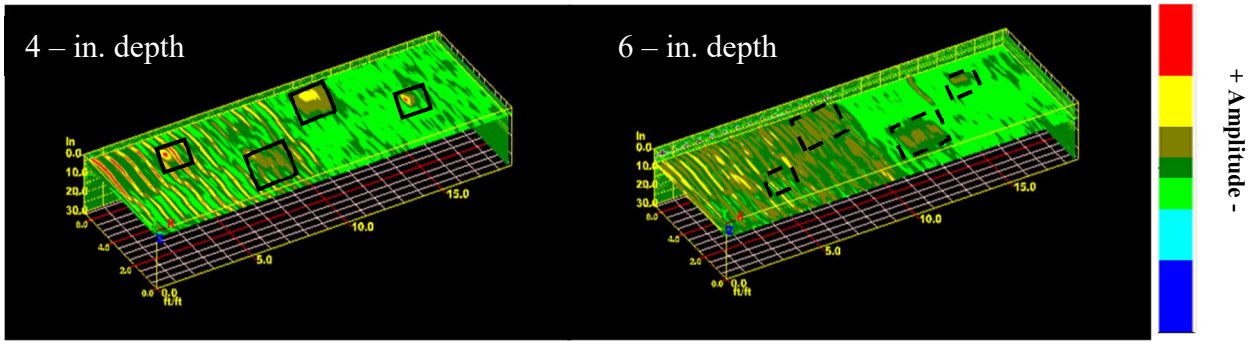

Day 250

Figure 5.10 – GPR 3D Models with Shallow and Deep Delaminated Areas

The contour maps of the propagation velocity of the electromagnetic waves with time are included in Figure 5.11. As time progresses, the electromagnetic velocity increases. Day 20 and Day 22 post-pouring show a dominant electromagnetic velocity distribution of 3 to 3.3 in./ns, while the later days of the specimen's concrete life (Days 109, 180, and 250) show a higher distribution of electromagnetic wave velocity with values between 3.5 to 4 in./ns. The increase in the velocity represents a shorter travel time with aging, effectively capturing the effect of the concrete hardenin

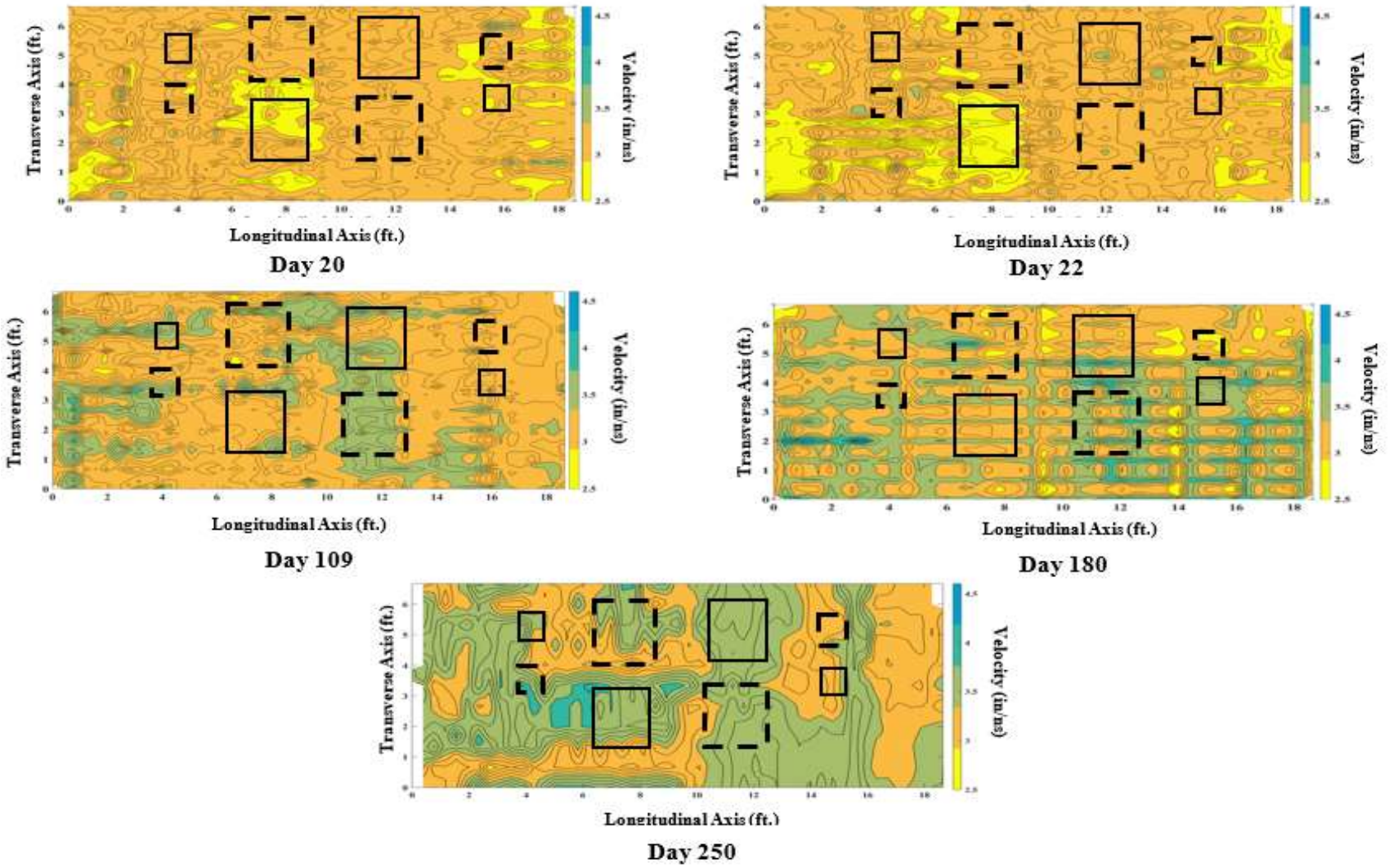

Figure 5.11 – GPR 3D Contours of Electromagnetic Velocity Distribution along the Concrete Sla

5.6 ELECTRICAL RESISTIVITY

The Wenner probe testing for resistivity was performed on days post-pouring: 1, 3, 7, 12, 16, 69, 157, 250 and 320. The bold dashed lined boxes represent the deep delaminated areas, while the thinner dashed lined boxes represent the shallow delaminated areas. The average resistivity of the concrete (excluding the delaminated areas) from the reinforced and non-reinforced area obtained from each test day are plotted with the error bars representing ±1 standard deviation in Figure 5.12. Due to the hardening condition of the concrete on Day 320, Wenner probe testing presented higher values of resistivity (from 250 - 1600 kΩ-cm) compared to the early days of the concrete specimen. For this reason, the data from day 320 were omitted in the figure to allow better visualization of the increase in resistivity during the early days.

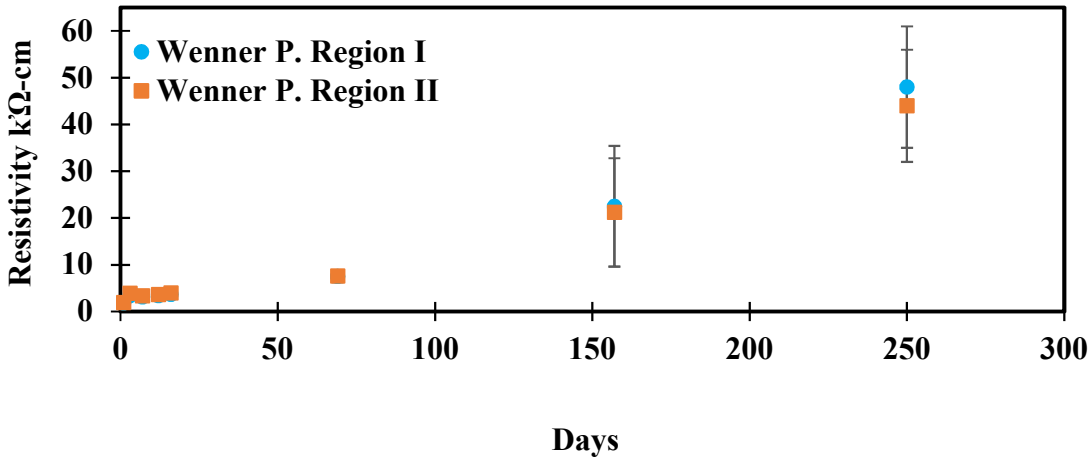

Figure 5.12 – Average Resistivity from Wenner Probe in Non-Delaminated Areas

The resistivity contours of the slab are shown in Figure 5.13. As expected, the resistivity increases with aging. Overall, it is observed that the Wenner probe is unsuccessful in detecting the delaminated areas due to the aridness and hardening of concrete over time that increases its resistivity and diminishes the probe's sensitivity to the high resistivity of the defects. However, Figure 5.13 does indicate that the Wenner probe did detect the plastic material of the shallow delaminated areas during the very early age of the concrete. For Day 1, at the location of the shallow defects and some of the deeper ones, the resistivity values are higher (as shown in yellow) indicating the probes ability to detect the defect's high resistivity cardboard material as compared to the wetter concrete. However, the process of delamination in fresh poured concrete is not common. The results from Day 1 are only detecting the material's (concrete vs plastic lined cardboard) resistivity differences. The Wenner probe, therefore, will show resistivity contrast when the concrete is exposed to actual humid climates, where these voids will be filled with water, and the corrosion process has progressed in the concrete specimen.

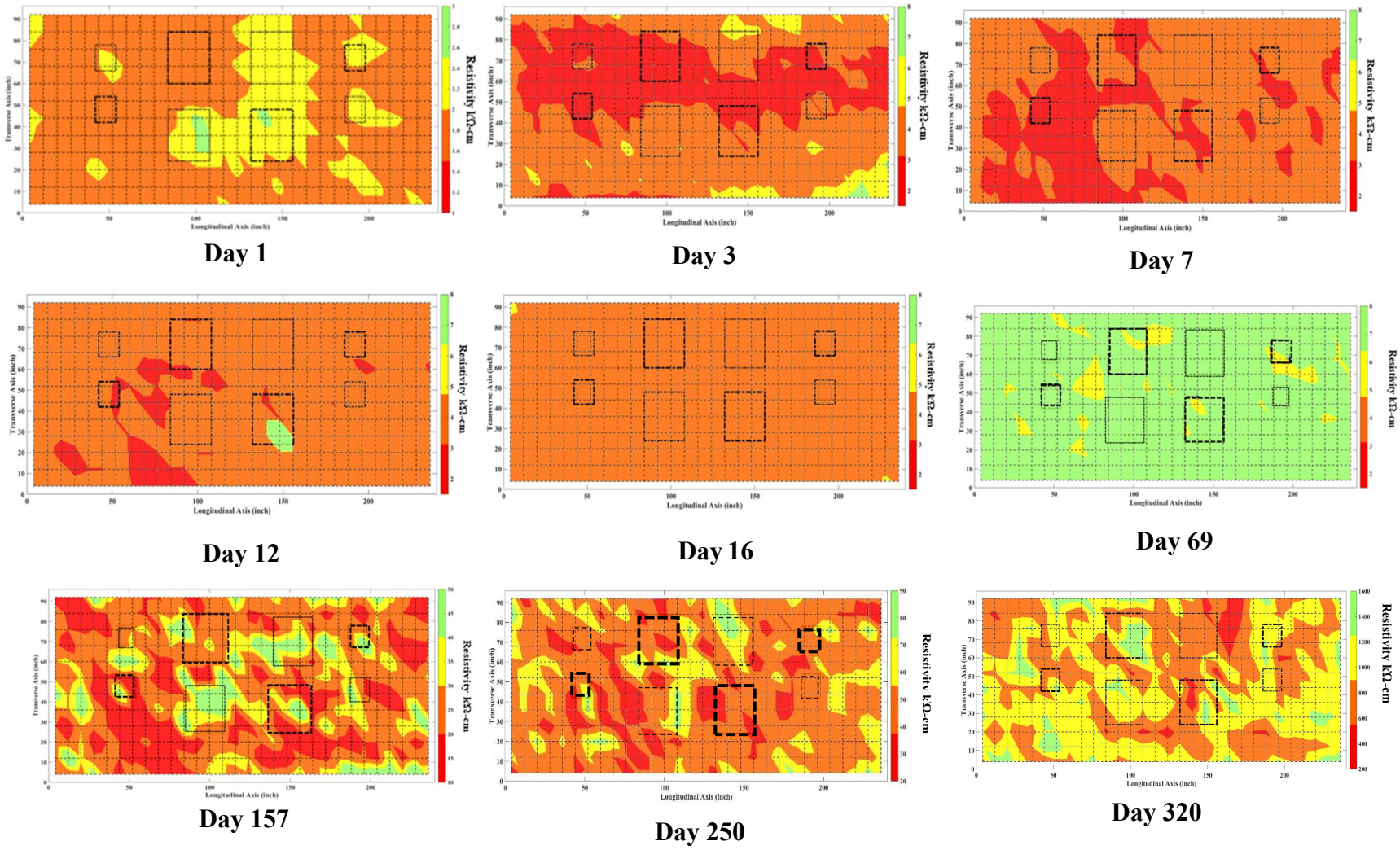

Figure 5.13 – Wenner Probe Resistivity Contours

Chapter 6: Summary and Conclusions

6.1 SUMMARY

A specimen built at The University of Texas at El Paso (UTEP) was tested utilizing various NDT tools to expand the knowledge and better understand the advantages and limitations of different NDT methods used for the detection of delamination in concrete bridge decks with aging. The NDT methods used for testing are: Portable Seismic Property Analyzer (PSPA), Ultrasonic Tomography (MIRA), Ground Penetrating Radar (GPR) and Resistivity Probe. These methods were applied to a slab containing both reinforced and unreinforced areas. Eight artificially delaminated areas of various sizes and depths were simulated through the use of 3-mm cardboard material lined with thin plastic. Data were collected regularly with each device over a 28-day span and then monitored thereafter in approximately three-month intervals. Below are the summarized results from each NDT method:

- Portable Seismic Property Analyzer (PSPA) could detect both shallow delaminated areas. The USW method consistently detected the shallow delaminated areas as the concrete aged, however the deep delaminated areas were not noticeable; only few deeper areas during the early days of the concrete's life were shown. The IE method detected the larger delaminated areas (both deep and shallow) as the concrete aged. The smaller delaminated areas were not always detected due to the limited number of measurements in each of these smaller areas. The smaller voids also don not reflect as much energy making them harder to detect.
- Ultrasonic Tomography (MIRA) was able to capture both deep and shallow delaminated areas, as well as the reinforcement throughout the concrete specimen's life. The transducer array MIRA possesses permits many pitch-catch, time-of-flight measurements to be made in a short period of time, and therefore the multiple reflections of this array configuration allow well defined reflections of these anomalies.

- Ground Penetrating Radar (GPR) could detect shallow delaminated areas efficiently during the early stages of the concrete specimen. As concrete aged, the areas were not as clearly identified. Deep delaminated areas were not as clearly distinguishable due to the obstructions or interfaces that cause a portion of the energy to be reflected back to the surface. GPR is able to capture the shallower reinforcement layer thoroughly with aging, while the deeper steel is not captured due to the large amount of energy that the shallower steel layer reflects back to the surface. The distribution of electromagnetic velocity along the slab was also analyzed as contours and the results showed that, as time progresses, the electromagnetic velocity increased.
- Resistivity Probe using a Wenner configuration was unsuccessful in detecting the delaminated areas with time. The aridness and hardening of the concrete loses moisture, creating higher resistivity values and decreasing the probe's ability to detect the difference between the concrete and the high resistivity voids.

6.2 RECOMMENDATIONS

It is recommended to pursue further research on several aspects of this study in order to broaden the scope of identifying the advantages and limitations of the NDT methods in detecting delamination in concrete bridge decks with aging. All technologies seemed to work efficiently in detecting certain defects. GPR is, however, limited in detecting delaminated areas due to the strong effect the metal reinforcement has in the electromagnetic wave propagation. USW also presents limitation in the detection of deeper delaminated areas. The Wenner Probe should be further evaluated. If voids were filled with water, better results might be obtained, as the actual chloride-ion induced corrosion of reinforcing steel would be better simulated and the actual areas of possible corrosion would be shown. Additionally, further research should be conducted on how the test procedures can be modified given cases of reinforcement presence in order to consistently identify defects beneath the rebar.

Appendix A

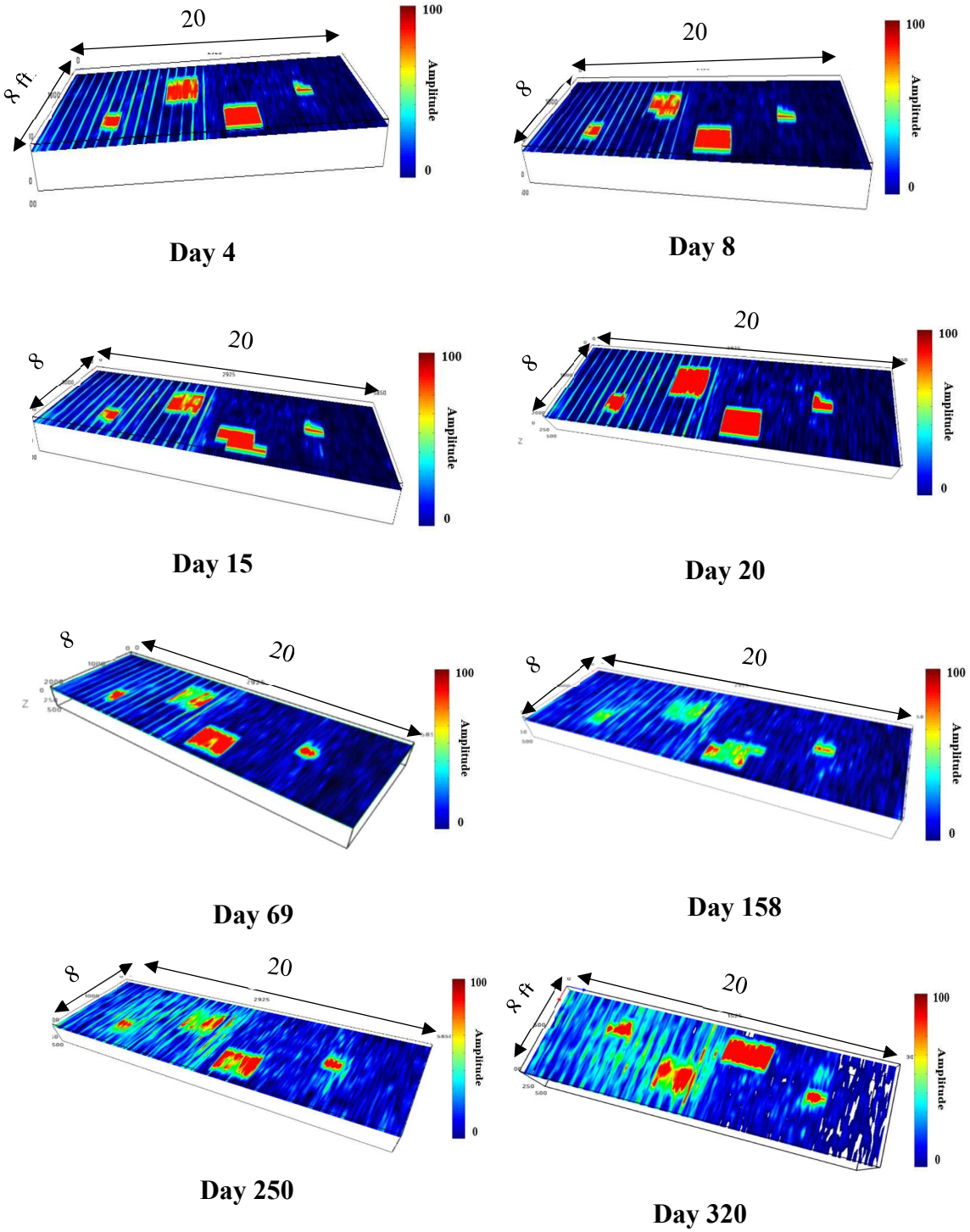

Figure A1 – MIRA 3D Shallow Delaminated Areas at a 4-in. depth

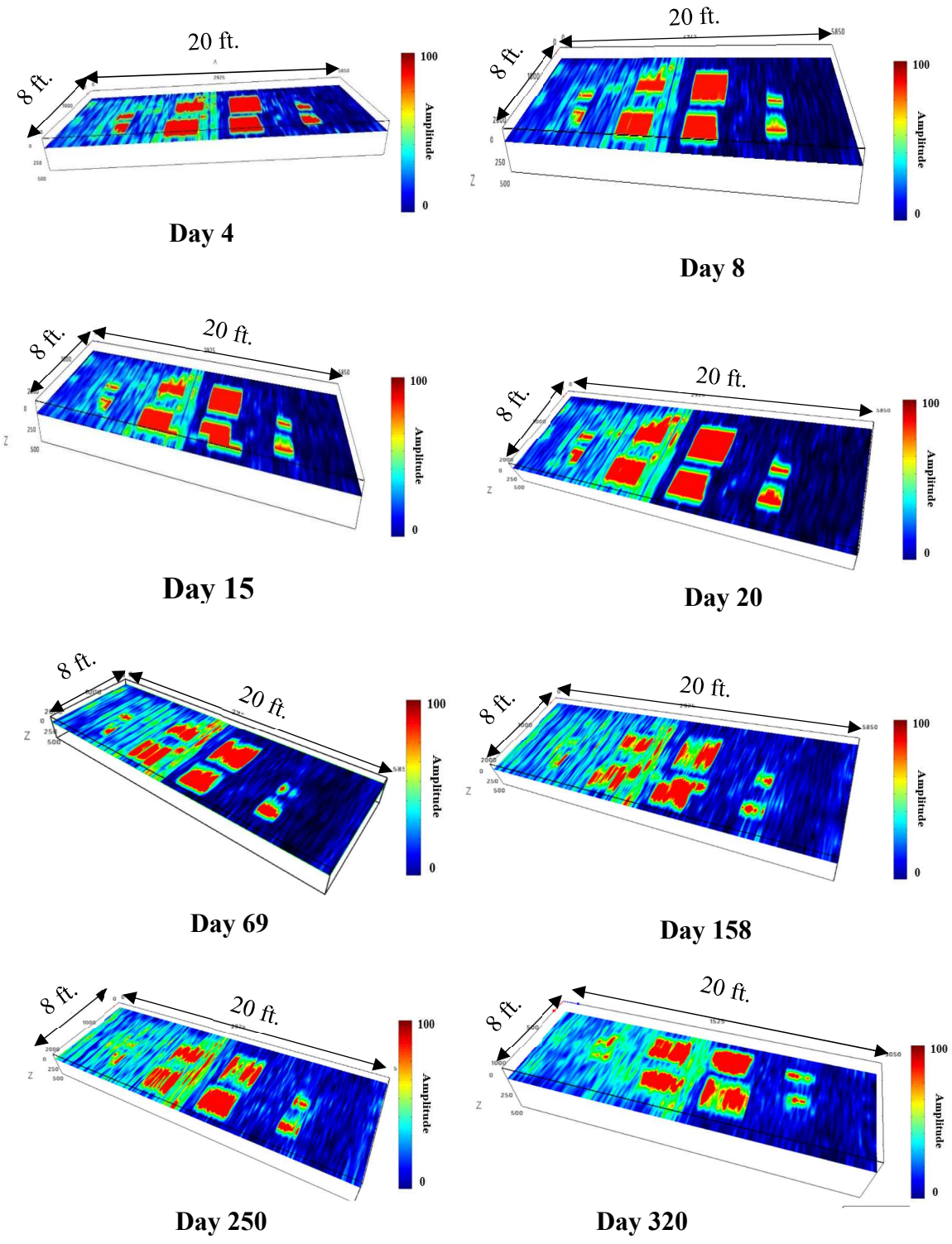

Figure A2 – MIRA 3D Shallow and Deep Delaminated Areas at a 6-in. depth

Points within the volume that have the same reflection amplitude are joined into groups which are called isosurfaces. The isosurfaces provided by the MIRA testing are shown in Figure 5.8. These surfaces represent points within a volume that have a constant reflection amplitude. The 3-D surfaces correspond to points with amplitudes above the selected threshold. This mode is helpful for estimating the real defect size above a given threshold value and for the detection of small inclusions. At the location of defects and reinforcement, the denser volume of constant reflection is evident, symbolizing the presence of these anomalies.

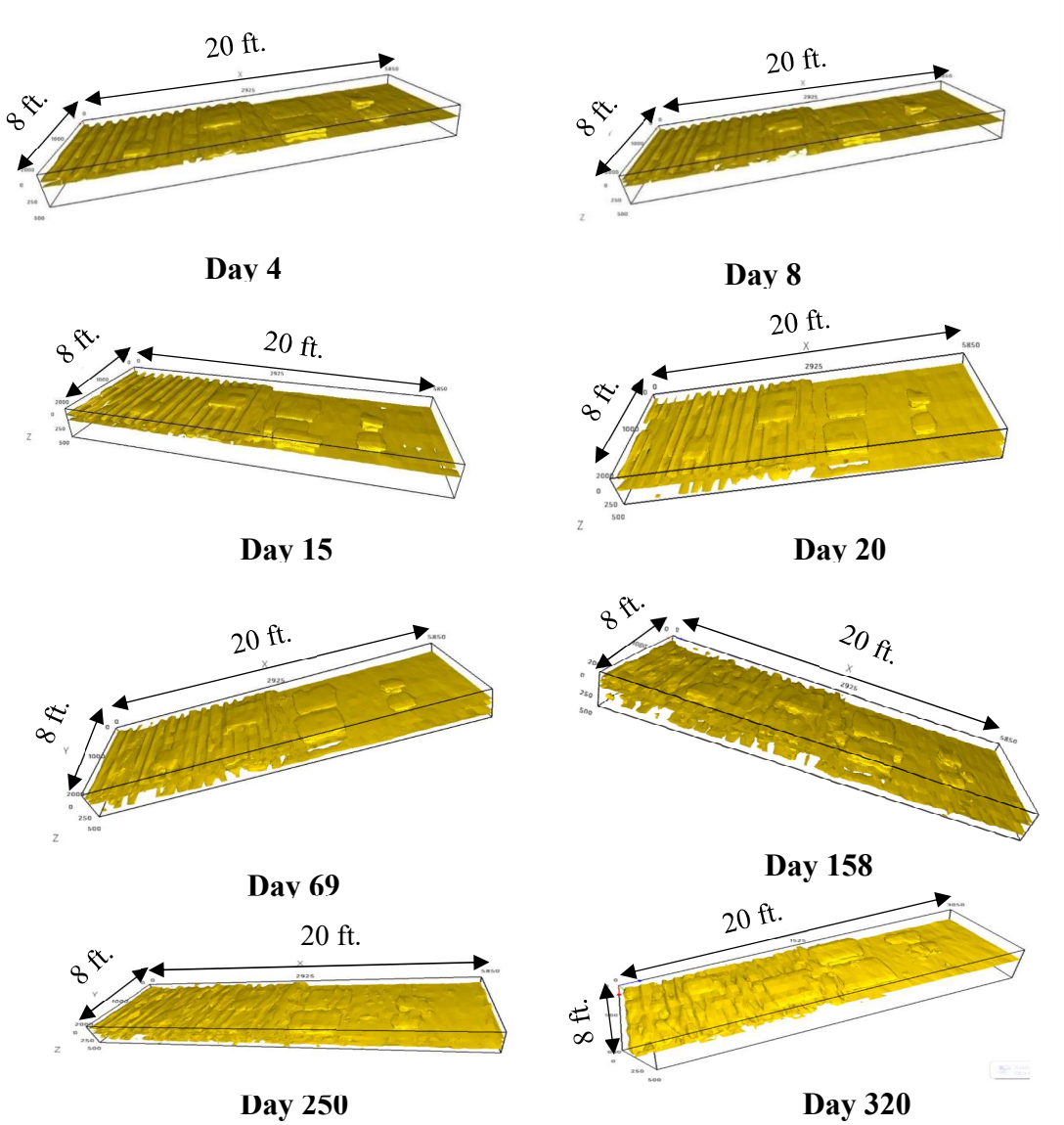

Figure A3 – MIRA Isosurface Contours at a 6-in. depth

References

Azari, H., Yuan, D., Nazarian, S., and Gucunski, N. (2012). "Impact of Testing Configuration and Data Analysis Approach on Detection of Delamination in Concrete Bridge Deck with Sonic Methods." Transportation Research Record (TRR): Journal of Transportation Research Board, 2292, 113-124.

Gowers, K. R., and S. G. Millard. 1999. Measurement of Concrete Resistivity for Assessment of Corrosion Severity of Steel Using Wenner Technique. ACI Materials Journal, Vol. 96 No. 5 pp. 536-542.

Gucunski, N. and Maher, A. (2000). "Bridge Deck Evaluation Using Portable Seismic Pavement Analyzer (PSPA)." Final Report, Report No. FHWA NJ 2000-05, Center for Advanced Infrastructure & Transportation (CAIT), Department of Civil & Environmental Engineering, the State University of New Jersey, Rutgers, NJ.

Gucunski, N., Imani, A., Romero, F., Nazarian, S., Yuan, D., Wiggenhauser, H., Shokouhi, P., Taffe, A. and Kutrubes, D. (2013). "Nondestructive Testing to Identify Concrete Bridge Deck Deterioration." SHRP 2 Report S2-R06-RR-1, the Second Strategic Highway Research Program, Transportation Research Board, Washington, D.C.

J. S. Popovics, J. R. Roesler, J. Bittner, A. N. Amirkhanian, A. S. Brand, P. Gupta, K. Flowers (2017). "Ultrasonic Imaging for Concrete Infrastructure Condition Assessment and Quality Assurance." University of Illinois at Urbana-Champaign, Federal Highway Administration, Report No. FHWA-ICT-17-007

J. White, S. Hurlebaus, P. shokouhi, A. Wimsatt. 2013. Use of Ultrasonic Tomography to Detect Structural Impairment in Tunnel Linings. Journal of the Transportation Research Board of the National Academies, Washington, D.C., No. 2407 pp. 20–31.

Maser, K. R. and Roddis, W. M. K. (1990). "Principles of Thermography and Radar for Bridge Deck Assessment." Journal of Transportation Engineering, Vol. 116, No. 5, pp. 583–601.

Miller, G. F. and Pursey, H. (1955). "On the Partition of Energy between Elastic Waves in a Semi-Infinite Solid." Proceedings of the Royal society of A: Mathematical, Physical and Engineering Scieneces, 233(1192), 55-69.

Romero, F.A., and R. L. Roberts. 20002. The Evolution in High-Resolution Ground Penetrating Radar Surveys from Ground-Coupled to High-Speed, Air-Coupled Evaluations. Proc., Structural Materials Technology V: An NDT Conference, Cincinnati, Ohio.

Vancura, M., L. Khazanovich, and R. Barnes. 2013. "Concrete Thickness Variation Assessment with Cores and Nondestructive Testing Measurements," Transportation Research Record, Issue 2347, pp. 61-68.

Washer, G., Fenwick, R., Bolleni, N., and Harper, J. (2009). "Effects of Environmental Variables on Infrared Imaging of Subsurface Features of Concrete Bridges." Transportation Research Record (TRR): Journal of Transportation Research Board, pp. 107- 114

Weyers, R. E., Prowell, B. D., Sprinkel, M. M., and Vorster, M. (1993). "Concrete Bridge Protection, Repair, and Rehabilitation Relative to Reinforcement Corrosion: A Methods

Application Manual." Strategic Highway Research Program Report No. SHRP-S-360, National Research Council, Washington, D.C.

Wimsatt, A., White, J., Leung, C., Scullion, T., Hurlebaus, S., Zollinger, D., Grasley, Z., Nazarian, S., Azari, H., Yuan, D., Shokouhi, P., Saarenketo, T., Tonon, F. (2012). "Mapping Voids, Debonding, Delaminations, Moisture, and other Defects Behind or Within Tunnel Linings." Preliminary revised draft final report, SHRP 2 Renewal Project R06-G, the Strategic Highway Research Program 2, Transportation Research Board of the National Academies.

Woods, R.D., (1968) "Screening of Surface Waves in Soils," Journal of the Soil Mechanics and Foundations Division, vol. 94, no. SM4, pp. 951-979.

Yuan, D., and Nazarian, S. (2000). "Feasibility of Detecting Flaws in Concrete Walls of Nuclear Power Plants." A report for Jet Propulsion Laboratory, California Institute of Technology, Center for Highway Materials Research, the University of Texas at El Paso.

Curriculum Vita

Melissa Escalante was born in El Paso, Texas on January 29, 1995. She graduated from Montwood High School in 2013. She joined The University of Texas at El Paso (UTEP) to complete her undergraduate degree in civil engineering. She was a recipient of the UTEP Presidential Excellence Scholarship and the National Science Foundation (NSF) Scholarship. During her undergraduate studies, she participated in different organizations, such as the American Society of Civil Engineers (ASCE) and Chi Epsilon - Civil Engineering Honor Society. During the summer of 2016, she had the opportunity to intern at the Texas Department of Transportation (TxDOT) at the El Paso District office. In the fall of 2016, Melissa began working as an undergraduate research assistant for the Center for Transportation Infrastructure Systems (CTIS), under the supervision of Dr. Soheil Nazarian. There she participated in projects involving the nondestructive evaluation of infrastructure. She received a Bachelor of Science in Civil Engineering degree, and graduated Summa Cum Laude in May, 2017. During the summer of 2017, she had the opportunity to intern at the United States Department of Transportation – Federal Highway Administration/Turner Fairbank Highway Research Center in McLean, VA where she worked in the Nondestructive Evaluation laboratory and the Petrographic laboratory. She also attended the Transportation Research Board (TRB) annual meeting as a Minority Student Fellow in January, 2018. She continued to serve as a graduate research assistant while pursuing a Master of Science in Civil Engineering with a focus in the nondestructive testing and evaluation of infrastructure.

Permanent address: PO Box 9525

El Paso, Texas, 79995

This thesis was typed by Melissa Escalante.